



UNIVERSITÉ LIBRE DE BRUXELLES

SUMMARY

**Aerodynamics
MECA-Y402**

Author:
Enes ULUSOY

Professor:
Herman DECONINCK

Year 2016 - 2017

Appel à contribution

Synthèse Open Source



Ce document est grandement inspiré de l'excellent cours donné par Herman DECONINCK à l'EPB (École Polytechnique de Bruxelles), faculté de l'ULB (Université Libre de Bruxelles). Il est écrit par les auteurs susnommés avec l'aide de tous les autres étudiants et votre aide est la bienvenue ! En effet, il y a toujours moyen de l'améliorer surtout que si le cours change, la synthèse doit être changée en conséquence. On peut retrouver le code source à l'adresse suivante

<https://github.com/nenglebert/Syntheses>

Pour contribuer à cette synthèse, il vous suffira de créer un compte sur *Github.com*. De légères modifications (petites coquilles, orthographe, ...) peuvent directement être faites sur le site ! Vous avez vu une petite faute ? Si oui, la corriger de cette façon ne prendra que quelques secondes, une bonne raison de le faire !

Pour de plus longues modifications, il est intéressant de disposer des fichiers : il vous faudra pour cela installer L^AT_EX, mais aussi *git*. Si cela pose problème, nous sommes évidemment ouverts à des contributeurs envoyant leur changement par mail ou n'importe quel autre moyen.

Le lien donné ci-dessus contient aussi un README contenant de plus amples informations, vous êtes invités à le lire si vous voulez faire avancer ce projet !

Licence Creative Commons

Le contenu de ce document est sous la licence Creative Commons : *Attribution-NonCommercial-ShareAlike 4.0 International (CC BY-NC-SA 4.0)*. Celle-ci vous autorise à l'exploiter pleinement, compte-tenu de trois choses :



1. *Attribution* ; si vous utilisez/modifiez ce document vous devez signaler le(s) nom(s) de(s) auteur(s).
2. *Non Commercial* ; interdiction de tirer un profit commercial de l'œuvre sans autorisation de l'auteur
3. *Share alike* ; partage de l'œuvre, avec obligation de rediffuser selon la même licence ou une licence similaire

Si vous voulez en savoir plus sur cette licence :

<http://creativecommons.org/licenses/by-nc-sa/4.0/>

Merci !

Contents

1 Aerodynamic Force	1
1.1 Derivation of the conservation laws	1
1.1.1 Mass conservation	1
1.1.2 Momentum equation	1
1.2 The aerodynamic lift	3
1.3 The Kutta-Joukowski formula	3
2 The 2D airfoil	5
2.1 Nomenclature	5
2.2 The flow around 2D airfoils	6
2.2.1 Distribution of the pressure coefficient	6
2.3 Center of pressure, moment and aerodynamic center	8
2.3.1 Center of pressure and moment	8
2.3.2 Aerodynamic center	9
2.4 2D characteristics	10
2.4.1 Lift, drag and moment curves	10
2.4.2 Stall and critical angle of attack	11
2.4.3 Maximum lift, stalling speed, polar curve and glide ratio	12
2.5 Methods to calculate flows around 2D airfoils	13
2.5.1 Conformal mapping	13
2.5.2 Thin airfoil theory	17
2.5.3 Numerical methods: source panel and vortex panel	22
3 The 3D wing	25
3.1 The downwash effect and the induced drag	25
3.1.1 Variation of the drag during the flight	27
3.2 Prandtl lifting line theory	27
3.2.1 Introduction : vortex lines and law of Biot-Savart	27
3.2.2 Prandtl lifting line formula	29
3.2.3 The elliptic lift distribution (application type II)	30
3.2.4 Wings with arbitrary distribution of the circulation	31
4 Viscous and turbulent effects	35
4.1 Skin friction	35
4.1.1 Laminar flow	35
4.1.2 Turbulent flow	36
4.2 Methods to reduce the drag	36
4.2.1 Natural laminar flow and control of laminar flow	36
4.2.2 Reduction of the drag in turbulent flows	37

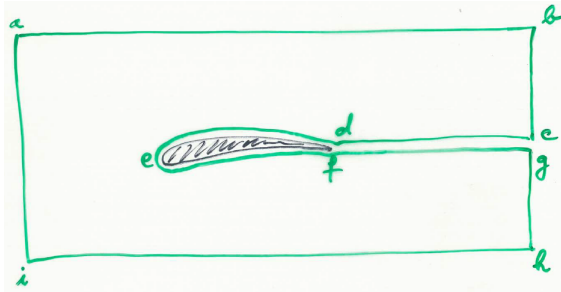
5 The complete plane: additional components	38
5.1 High lift devices	38
5.1.1 Trailing edge flaps	38
5.1.2 Slat	39
5.1.3 Leading edge flap	40
5.2 Boundary layer control	40
5.3 Tailplanes	40
6 2D wings in compressible flow	42
6.1 Subsonic flows	42
6.1.1 The Prandtl-Glauert relation	42
6.1.2 Improved corrections for compressibility	45
6.1.3 The critical Mach number	46
6.2 Transonic flows	47
6.2.1 Drag divergence Mach number	47
6.2.2 Supercritical wings	49
6.3 Supersonic flows	49
6.3.1 The drag coefficient in a linearized supersonic flow	49
6.3.2 Supersonic wings	52
7 3D wings in compressible flows	54
7.1 The Prandtl-Glauert-Goethert transformation	54
7.1.1 Subsonic flows	54
7.1.2 Supersonic flows	55
7.2 Swept wings	55
7.2.1 Lift of swept wings	55
7.2.2 Lift coefficient as a function of the angle of attack for swept wings	56
7.2.3 Influence of the sweep angle on the drag	56
7.2.4 Some additional disadvantages of wings	56
7.3 Area rule	58
7.4 Delta wings	59

Chapter 1

Aerodynamic Force

1.1 Derivation of the conservation laws

1.1.1 Mass conservation



Consider the closed control volume S^* (abhi) around the airfoil. It is a 2D view, but imagine that we have a 3D configuration with Z axis perpendicular to the sheet. Be aware that the normal is always perpendicular to the contour and is external! The fundamental integral form of the mass conservation equation is:

Figure 1.1

$$\frac{d}{dt} \int_V \rho dV + \oint_S \rho \vec{v} d\vec{S} = 0. \quad (1.1)$$

By applying Gauss theorem $\oint_S \vec{a} \cdot \vec{n} dS = \int_V \nabla \cdot \vec{a} dV$, and regrouping the term in a unique integral, we obtain:

$$\int_V \left[\frac{d\rho}{dt} + \nabla \cdot (\rho \vec{v}) \right] dV = 0. \quad (1.2)$$

Considering this to be true for all volumes, the integral disappear and gives the

Continuity equation

$$\frac{d\rho}{dt} + \nabla \cdot (\rho \vec{u}) = 0 \quad (1.3)$$

Another form can be found by introducing the material derivative $\dot{\rho} = \frac{d\rho}{dt} + (\vec{v} \cdot \nabla) \rho$, and if we are in a steady state, the time derivative goes away.

1.1.2 Momentum equation

The general form of the momentum equation is:

$$\rho \dot{\vec{v}} = \frac{\partial \rho \vec{v}}{\partial t} + \rho (\vec{v} \nabla) \vec{v} = -\nabla p + \nabla \bar{\tau}. \quad (1.4)$$

By considering a steady state, the time derivative goes away. If we consider the x component of the velocity, we can expend the derivative to the whole left term as:

$$\rho(\vec{v}\nabla)v_x = \nabla(\rho\vec{v}v_x) - v_x\nabla(\rho\vec{v}) \quad (1.5)$$

where the last term is null related to (1.3) in steady state. Integrating both sides around the volume contained in the closed surface S (abcdefghi on figure) in (1.5), and applying Gauss theorem, we obtain:

$$\oint_S \vec{v}(\rho\vec{v}\vec{n}) dS = - \oint_S p d\vec{S} + \oint_S \bar{\tau} d\vec{S}. \quad (1.6)$$

Let's now apply this equation to the new closed contour $S^* = S - \text{airfoil} - cd - fg$ (previous abhi in fact). (1.6) becomes:

$$\begin{aligned} & \oint_{S^*} \vec{v}(\rho\vec{v} d\vec{S}) + \oint_{\text{airfoil}} \vec{v}(\rho\vec{v} d\vec{S}) + \oint_{cd+fg} \vec{v}(\rho\vec{v} d\vec{S}) \\ &= - \oint_{S^*} p d\vec{S} - \oint_{\text{airfoil}} p d\vec{S} - \cancel{\oint_{cd+fg} p d\vec{S}} + \oint_{S^*} \bar{\tau} d\vec{S} + \oint_{\text{airfoil}} \bar{\tau} d\vec{S} + \cancel{\oint_{cd+fg} \bar{\tau} d\vec{S}} \end{aligned} \quad (1.7)$$

where the $cd + fg$ components cancels each other if we consider that they are infinitely close to each other, as they are opposite. The airfoil integral in the left hand side is null because the wing can not be penetrated by the flow. If we manipulate the equation to refind the (1.6) shape by regrouping airfoil terms in an additional \vec{R} term. Taking account the orientation of normals, the signs will be chosen in the way \vec{R} is a

Force applied on the wing

$$\vec{R} = \oint_{\text{airfoil}} p d\vec{S} - \oint_{\text{airfoil}} \bar{\tau} d\vec{S} \quad (1.8)$$

so that (1.7) becomes, after considering S^* to be a contour in the **far field** so that viscous effects vanish (to avoid other parameters calculation):

$$\oint_{S^*} \vec{v}(\rho\vec{v} d\vec{S}) = - \oint_{S^*} p d\vec{S} + \oint_{S^*} \bar{\tau} d\vec{S} - \vec{R}. \quad (1.9)$$

We still have to measure the pressure.

Uniform p along S^*

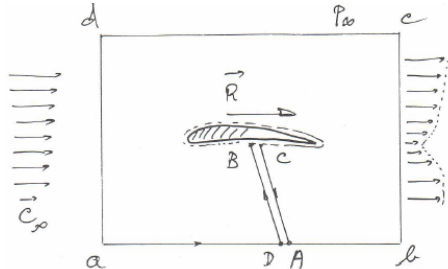


Figure 1.2

horizontal so that $\vec{R} = R\vec{1}_x$, at the inlet we have \vec{v} and \vec{n} are opposed while at the outlet they are in the same direction:

$$\vec{R} = \int_a^d \vec{v} dm - \int_b^e \vec{v} dm > 0 \quad (1.11)$$

showing that there is only **drag** force.

1.2 The aerodynamic lift

We know in practice that there is also a lift force. In fact, the assumption of uniform pressure is wrong because the pressure effects induced by the body remains at a long distance from the body. We have to analyse the **non uniform** p along S^* . In order to apply Bernouilli equation $p + \frac{1}{2}\rho v^2 = cst$, let's add the constants p_∞ and v_∞ to (1.9), as $\oint p_\infty d\vec{S} = p_\infty \oint d\vec{s} = 0$:

$$\vec{R} = - \oint_{S^*} (p - p_\infty) d\vec{S} - \oint_{S^*} (\vec{v} - \vec{v}_\infty) d\dot{m} \quad (1.12)$$

Let's express $\vec{v} = \vec{v}_\infty + \vec{\delta}_c$ with $\vec{\delta}_c$ a perturbation. Introducing this in Bernouilli equation:

$$\begin{aligned} p_\infty + \frac{1}{2}\rho \vec{v}_\infty^2 &= p + \frac{1}{2}\rho(\vec{v}_\infty + \vec{\delta}_c)^2 = p + \frac{1}{2}\rho(\vec{v}_\infty^2 + 2\vec{v}_\infty \cdot \vec{\delta}_c + \vec{\delta}_c^2) \\ &\Rightarrow p - p_\infty = -\rho \vec{v}_\infty \cdot \vec{\delta}_c. \end{aligned} \quad (1.13)$$

If we replace this result in (1.12), we find:

$$\begin{aligned} \vec{R} &= \oint_{S^*} \rho(\vec{v}_\infty \cdot \vec{\delta}_c) d\vec{S} - \oint_{S^*} \rho \vec{\delta}_c [(\vec{v}_\infty + \vec{\delta}_c) d\vec{S}] \\ &= \oint_{S^*} \rho [(\vec{v}_\infty \cdot \vec{\delta}_c) d\vec{S} - \vec{\delta}_c [(\vec{v}_\infty \cdot d\vec{S})]] \end{aligned} \quad (1.14)$$

by using a vector property $\vec{a} \times (\vec{b} \times \vec{c}) = (\vec{a} \cdot \vec{b})\vec{c} - (\vec{a} \cdot \vec{c})\vec{b}$:

$$= \rho \vec{v}_\infty \times \oint_{S^*} \vec{\delta}_c \times d\vec{S} = \rho \vec{v}_\infty \times \left[\oint_{S^*} \vec{v} \times d\vec{S} - \oint_{S^*} \vec{v}_\infty \times d\vec{S} \right] \quad (1.15)$$

and by applying Stokes theorem $\oint_S \vec{a} \times d\vec{S} = \int_V \nabla \times \vec{a} dV$:

$$= \rho \vec{v}_\infty \times \int (\nabla \times \vec{v}) dV = \rho \vec{v}_\infty \times \int \vec{\omega} dV \quad (1.16)$$

where $\vec{\omega}$ is the **vorticity vector** of direction \vec{I}_z (pointing in the paper):

$$\vec{\omega} = \begin{vmatrix} \vec{I}_x & \vec{I}_y & \vec{I}_z \\ \partial_x & \partial_y & 0 \\ v_x & v_y & 0 \end{vmatrix} = [\partial_x v_y - \partial_y v_x] \vec{I}_z \quad (1.17)$$

This shows that the lift force is always perpendicular to the flow!

1.3 The Kutta-Joukowski formula

We will now introduce the circulation $\Gamma = -\oint \vec{v} d\vec{l} > 0$ around a body. The convention is to take the anticlockwise direction for $d\vec{l}$ and so for Γ to be > 0 we must have \vec{v} in the clockwise direction. There is a link between the lift force and the circulation. Let's introduce **Stokes theorem**:

$$\oint \vec{a} d\vec{l} = \int_S (\nabla \times \vec{a}) d\vec{S} \quad \Rightarrow -\Gamma = \int_S \vec{\omega} d\vec{S}. \quad (1.18)$$

We remember that:

$$\begin{aligned} \vec{R} &= \rho \vec{v}_\infty \times \int \vec{\omega} dV = \rho \vec{v}_\infty \times \int l \vec{\omega} dS \quad \Leftrightarrow \frac{\vec{R}}{l} = \rho \vec{v}_\infty \times \int \vec{\omega} dS \\ \frac{\vec{R}}{l} &= \rho \vec{v}_\infty \times \int \vec{\omega} (d\vec{S} \cdot \vec{I}_z) = \rho \vec{v}_\infty \times (-\Gamma) \vec{I}_z = \rho v_\infty \Gamma \vec{I}_y \end{aligned} \quad (1.19)$$

to finally obtain a very good approximation of the lift:

Kutta formula for lift 2D airfoil

$$|R| = \rho v_\infty \Gamma \quad (1.20)$$

Application to airfoils

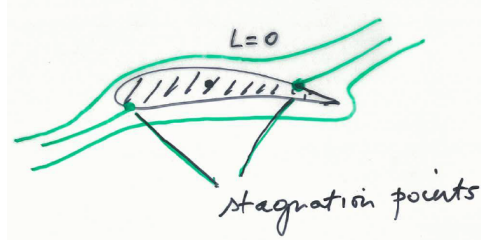


Figure 1.3

In inviscid case, the Kelvin theorem states that there cannot be vorticity, so no lift. If we take an arbitrary contour around the airfoil we will have no circulation. In inviscid case we can never get a lift \rightarrow D'alembert paradox. At the trailing edge, if the flow wants to continue on the other corner from below, the velocity must be infinity so that the flow separates. But this is not the case in reality.

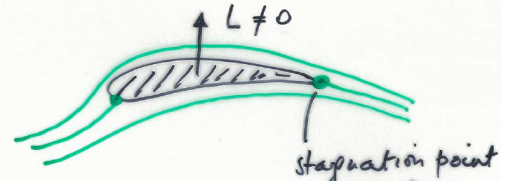


Figure 1.4

After some processes we can obtain the stagnation point on the trailing edge so that we satisfy the Kutta condition (the flow has to leave the airfoil smoothly). So in this case, there is a circulation if we take a contour that contains the airfoil, but for all contour that does not contain the airfoil it is null. But why to put the stagnation point at the trailing edge? This is purely physics. Γ varies with the stagnation point position, but only one corresponds to the Kutta condition.

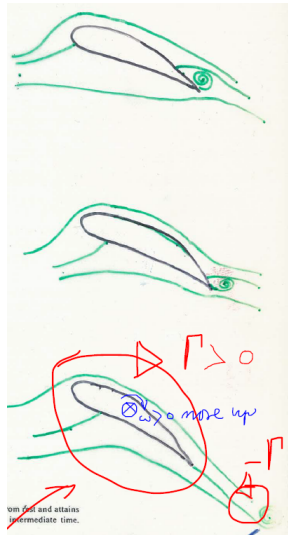


Figure 1.5

What happens is that initially we have the first kind of flow, then the formation of the starting vortex due to viscous effects (separation) which is compensated by a **bound vortex** around the airfoil (to respect Kelvin theorem of irrotational flow) that makes $\Gamma \neq 0$. Then the vortex goes away to infinity. Indeed if we take $R = \rho v_\infty \Gamma$, $\Gamma \neq 0$, so we have lift.

We can show that every contour containing the airfoil has a non 0 circulation. Let's proof that a contour that doesn't contain the airfoil has $\Gamma = 0$:

ADD FIGURE (1)

$$\oint_C \vec{v} d\vec{l} = \oint_{\text{airfoil}} \vec{v} d\vec{l} + \oint_{cd} \vec{v} d\vec{l} + \oint_{fg} \vec{v} d\vec{l} = 0. \quad (1.21)$$

As the contour elements are exactly opposed to each other, the result is null.

Chapter 2

The 2D airfoil

2.1 Nomenclature

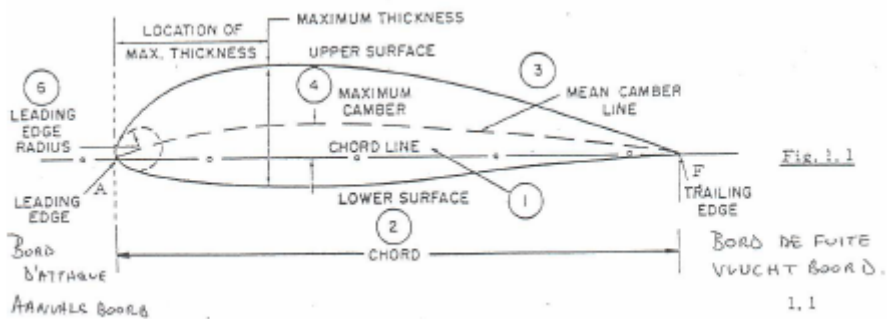


Figure 2.1

The connection between the trailing edge and the leading edge is called the **chord**. Then we have a **camber line** which is the line following the shape of the airfoil and characterizing the geometry. The leading and trailing edges are respectively the starting and ending point of the camber line. The thickness is always normal to the camber line. Let's note that the camber line and the thickness distribution are function of the position $f(x)$.

Eastman Jacobs created around 1930 a family of wing profiles, known as the NACA profiles. He characterised them by 4 digit numbers:

- The first is the **maximum camber in percentage of the chord**
- The second is the **position of the maximum camber in 1/10 percentage of the chord**
- The last two digits gives the **position of the maximum thickness in percentage of the chord**

These were characterizing the 2D representation, but a wing is 3D. We have also the **wing surface S**, the **span of the wing b** and we can define a mean chord when this last is not constant as:

$$\langle c \rangle = \frac{S}{b}. \quad (2.1)$$

For civil aircraft, b/c is between 6-10 and for glider $b/c = 12$, this is called the **aspect ratio** (slenderness ratio).

2.2 The flow around 2D airfoils

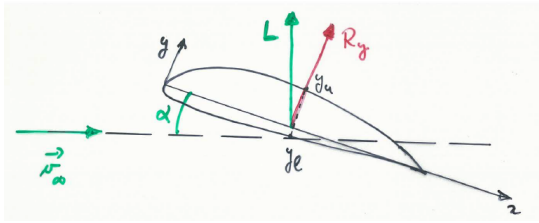


Figure 2.2

friction term is responsible for drag. Friction forces work tangential to the airfoil and the pressure forces are perpendicular, if there is **no separation** in the flow. The drag created by the stress is called the **skin or friction** drag. Note that in a subsonic inviscid incompressible flow, we have the paradox of d'Alembert because we have no drag. This shows that the pressure only contributes to lift.

What happens when we have **separation** is that we have a region above the airfoil where $p - p_\infty \approx 0$ and so we have a very big pressure below $p \gg p_\infty$ that slows down the wing. This implies that the applied force is higher than the case without separation and due to the attack angle, the drag force too. This phenomenon is called **pressure drag** (form drag), and here the pressure contributes to drag.

ADD FIGURE 4

The figure shows how the geometry of the body influence the drag force which can be sometimes principally caused by pressure. If we have a flat plate or a cylinder we have a huge separation, so principally a form drag D_f . We will have less pressure drop with the wing profile as it perfectly follows the flow direction, to end up smoothly, in this case the friction drag D_f is more important. This shows the importance of profiles.

If we look to the weight of a plane, it is surprising to see the importance of lift force. This is possible thanks to the high **atmospheric pressure**. Indeed, the wing load is defined as:

$$\text{wing load} = \frac{\text{weight plane}}{\text{surface area wings}} \quad (2.3)$$

and this is commonly approximately equal to $5000 \text{ Pa} = 500 \text{ kg/m}^2$. This can be easily reached by a small perturbation of the atmospheric pressure ($10^5 \text{ Pa} \rightarrow 5\% = 5000 \text{ Pa}$).

2.2.1 Distribution of the pressure coefficient

Let's see the effect of the angle of attack. For small angles, we can neglect the force derivation implied and consider it to be perpendicular to the chord. This allows to neglect the

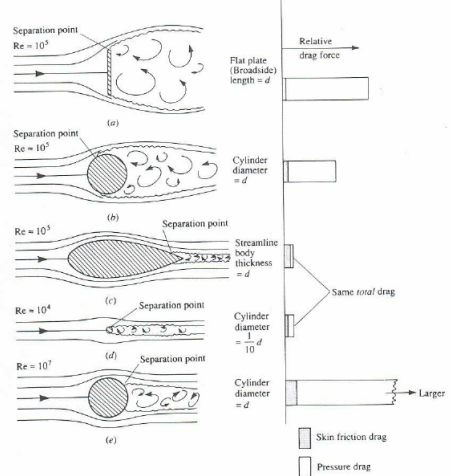


Figure 2.3

drag component (refer to Figure 2.2). If we assume that v is in the x direction, the lift force approximation is:

$$R_y = - \oint p d\vec{S} \cdot \vec{1}_y = - \oint p dS_y. \quad (2.4)$$

The lift force is fully created by pressure and we can call the lower part of the wing the **pressure side** and the upper part the **suction side**.

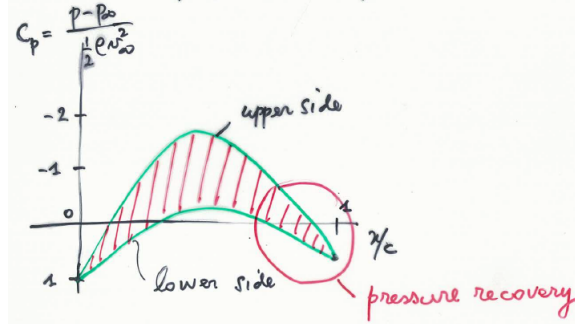


Figure 2.4

account the stagnation point where $v = 0$, we have:

$$p_\infty + \rho \frac{v_\infty^2}{2} = cst = p_{LE} + 0 \quad \Rightarrow C_p = \frac{p_{LE} - p_\infty}{\frac{1}{2} \rho v_\infty^2} = 1. \quad (2.5)$$

The pressure recovery means that we will have again $p = p_\infty$ at that point. At the leading edge this is the case because it is commonly a stagnation point.

For the trailing edge we have two cases. If it is **blunt** trailing edge, we have the $C_p = 1$ case (leading edge always blunt). If we have a **sharp** trailing edge, we will have v_∞ at the previous stagnation point and so the Bernouilli equation rewrites:

$$p_\infty + \rho \cancel{\frac{v_\infty^2}{2}} = cst = p_{TE} + \rho \cancel{\frac{v_\infty^2}{2}} \quad \Rightarrow C_p = \frac{p_{TE} - p_\infty}{\frac{1}{2} \rho v_\infty^2} = 0. \quad (2.6)$$

We have a very big expansion on the LE (separation), so this induces a suction peak as the pressure falls above and increases below. Then we go back to the normal pressure. Let's remind that decreasing pressure is favourable because the flow stays attached but if we have pressure increase, it's unfavourable, because we risk separation. The angle of attack is important because the flow has more difficulties to turn on the LE when angle goes up so the separation and the sucking peak are more important.

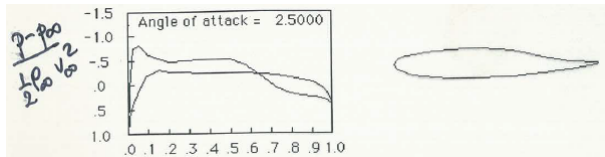
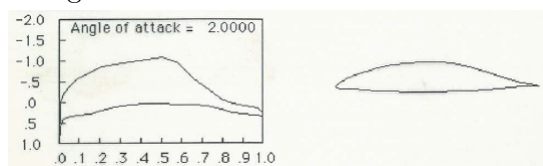


Figure 2.5

This case is particular because the rear is reversed, so the pressure side becomes sucking and inversely. The reduced camber and reduced thickness makes the wing more vulnerable to angle change.



Natural laminar section. The smoother LE reduces the peak and the sharp TE induces $C_p = 0$.

Figure 2.6

This is a symmetrical shape and thus only one line is shown. The thickness makes it more resistible to angle change.

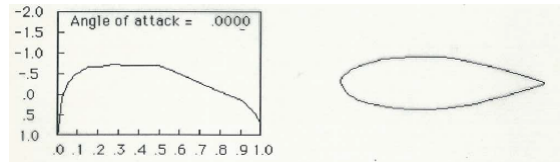


Figure 2.7

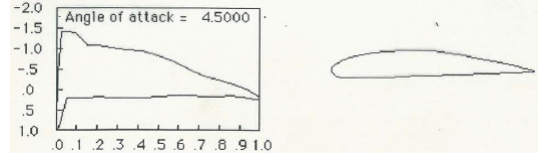


Figure 2.8

Even if the wing is thin, the camber makes it more suited to high attack angle.

2.3 Center of pressure, moment and aerodynamic center

2.3.1 Center of pressure and moment

Calculation of lift force

We can calculate the lift by $L = \rho v_\infty \Gamma$, but we need the Γ which is not calculable. So we will use the trick that consist in forgetting the drag term in the \vec{R} . Then we integrate the pressure around the surface:

$$\vec{R} = - \oint p d\vec{S} = - \sum_{\Delta R_i} \underbrace{p_i \Delta \vec{S}_i}_{\Delta R_i} \quad (2.7)$$

Center of pressure

It's the x value on the chord where the carrier of the force \vec{R} intersects the chord. It's function of the angle of attack. Indeed, if alpha increases, the suction peak will be higher, this induces that the center of pressure move forward (participation of the forward pressure more important).

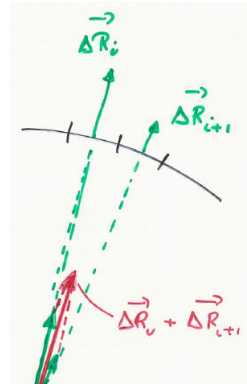
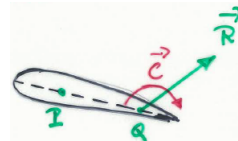


Figure 2.9

Note that the center of pressure is not a fixed point. Indeed, it varies with the angle of attack: if $\alpha \nearrow$, the pressure peak on the LE is more important making the x_p move upstream, and the contrary for $\alpha \searrow$. This notion will be completed by the **zero lift angle** α_0 .

Equivalent forces



The force at the pressure center P is equivalent to another force in point Q, but by adding the moment to compensate the one added by moving the force. This moment is:

$$\vec{C}_Q = -\vec{P}\vec{Q} \times \vec{R}. \quad (2.8)$$

Figure 2.10

Aerodynamic center

Suppose that there is a point Q where this couple C_Q is independent of the angle of attack (because the pressure center changes with alpha). This point is called the aerodynamic center. We have to show that this exists. For this way:

1. We will begin by calculating the center of pressure by integrating the pressure field. We can calculate the magnitude, but not the acting point.

2. We compute the momentum of the pressure forces around the leading edge (Figure 2.11):

$$\vec{M}_{LE} = \oint O\vec{Q} \times d\vec{F} = \underbrace{M_{LE}}_{<0} \vec{1}_z \quad (2.9)$$

where $\vec{1}_z$ goes in the paper.

3. On the other hand, we know that \vec{R} has a certain direction with a normal component, so we can make the moment (Figure 2.12):

$$M_{LE} = -x_p.N \quad (2.10)$$

By using point 2 and 3 we can find x_p .

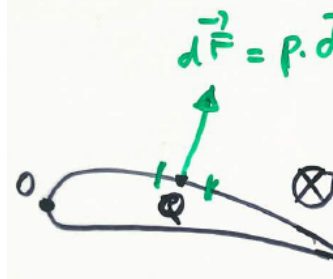


Figure 2.11

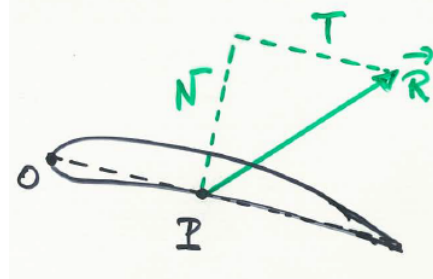


Figure 2.12

2.3.2 Aerodynamic center

Let's now be interested in how the moment on a point Q on the wing varies with α . It is shown experimentally that:

$$c_m(Q) = c_{m0} + kc_l \quad (2.11)$$

where c_m, c_l are respectively the non-dimensional moment and lift, and c_{m0} the non-dimensional moment at zero lift. k is a constant that is related to the reference point chosen. If Q is taken on the LE for example, increasing α will produce an increase of the lift and make the center of pressure move upstream. The L increase will compensate the moving x_p such that the moment becomes even more nose-down (more negative following $\vec{1}_z$) $\Rightarrow k < 0$ for a decrease in (2.11). The same reasoning applied on the trailing edge gives $k > 0$.

This shows that it exists a point where $k = 0$, called the **aerodynamic center**. According to (2.11), this point will have a constant moment whatever α . Indeed, we will show that $c_l = m(\alpha - \alpha_0)$ and so:

$$c_m(Q) = c_{m0} + km(\alpha - \alpha_0) \Rightarrow c_m(Q) = c_{m0}. \quad (2.12)$$

We can benefit from this equation to show that c_{m0} is well the moment for $\alpha = \alpha_0$, the zero lift angle (negative, descending arrow). We will also later show that when we decrease the angle of attack beginning from a positive one to the zero lift angle, the x_p will go downstream till infinity away the trailing edge, with an infinitely small lift,. This means that we will always have a finite nose-down moment.

Taking the opposite case of beginning from negative value of α , we will have the same value since the lift force is negative and the x_p in infinity further away from the leading edge. The **moment at zero lift** is thus **negative**. The explanations lead to the figures below.

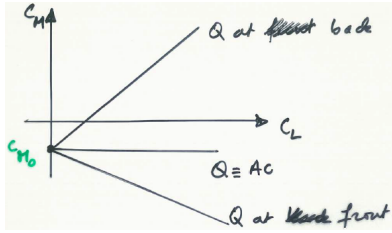


Figure 2.13

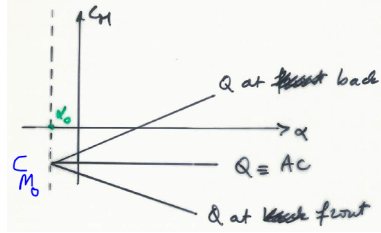


Figure 2.14

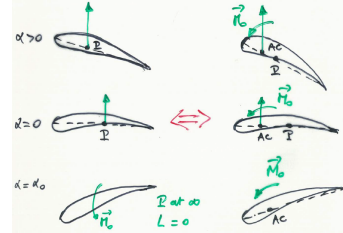


Figure 2.15

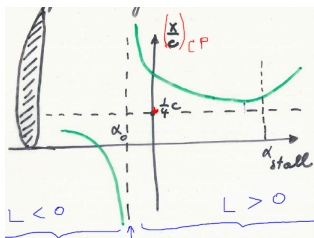


Figure 2.16

Let's finally establish the evolution of the pressure center in function of α . For this purpose, we need 4 equations:

$$\begin{aligned} 1) \quad c_m &= c_{m_0} + kc_l & 2) \quad M_{ac} &= (x_{ac} - x_{cp})N \\ 3) \quad m_{ac} &= M_{AC} = M_0 < 0 & 4) \quad N &= n(\alpha - \alpha_0) \end{aligned} \quad (2.13)$$

The AC being always upstream the CP the difference in 2) is < 0 . In 4), $n > 0$. By using equation 3,4 and 2, we can compute:

$$M_0 = -(x_{cp} - x_{ac}).n(\alpha - \alpha_0) \Leftrightarrow -\frac{M_0}{n} = (x_{cp} - x_{ac}).(\alpha - \alpha_0) \quad (2.14)$$

This is the equation of an **hyperbola**. To see it, we only have to compute the limits of:

$$\begin{aligned} x_{cp} &= x_{ac} - \frac{M_0}{n} \frac{1}{\alpha - \alpha_0} \\ \lim_{\alpha \rightarrow \pm\infty} x_{cp} &= x_{ac} \quad \lim_{\alpha \rightarrow \alpha_0 > 0} x_{cp} = +\infty \quad \lim_{\alpha \rightarrow \alpha_0 < 0} x_{cp} = -\infty \end{aligned} \quad (2.15)$$

The graph is shown on figure. Let's finally say that commonly, $x_{ac} = cst \approx \frac{1}{4}C$.

A particular case is the one of **symmetrical profile**. Indeed, in that case, the α_0 case correspond to $M_{ac} = 0$ and $L = 0$. The pressure center corresponds with the aerodynamic center and is **fixed**.

2.4 2D characteristics

2.4.1 Lift, drag and moment curves

Let's look to the non-dimensional parameters that will influence the lift;, the drag and the momentum. We have to define some reference quantities:

$$\begin{aligned} L_{ref} &= C & v_{ref} &= v_\infty & t_{ref} &= L_{ref}/v_{ref} & \rho_{ref} &= \rho_\infty \\ t' &= t/t_{ref} & p_{ref} &= \rho_{ref} \frac{v_{ref}^2}{2} & \text{Mach} &= V_{ref}/a_{ref} & a_{ref} &= \gamma \pi T_{ref} \\ \gamma &= c_p/c_v & Re_{ref} &= \frac{\rho_{ref} v_{ref} L_{ref}}{\mu_{ref}} \end{aligned} \quad (2.16)$$

where a is the speed of sound. By replacing all these in the mass, momentum and energy equations, we obtain the non-dimensional ones (see Fluid Mechanics II):

$$\begin{aligned}
& \bullet \frac{\partial \rho'}{\partial t'} + \nabla (\rho' \vec{v}') = 0 \\
& \bullet \rho' \frac{d\vec{v}'}{dt'} = -\frac{1}{\gamma M_{ref}^2} \nabla p' + \frac{1}{Re_{ref}} \nabla \bar{\tau}' \\
& \bullet \frac{d}{dt'} (\rho' e') + \frac{\gamma(\gamma-1)}{2} M_{ref}^2 \frac{d}{dt'} (\rho' \vec{v}'^2) \\
& = \frac{\gamma}{Pr_{ref} Re_{ref}} \nabla (k' \nabla T') - (\gamma-1) \nabla (p' \vec{v}') + \gamma(\gamma-1) \frac{M_{ref}^2}{Re_{ref}} \nabla (\bar{\tau}' \vec{v}')
\end{aligned} \tag{2.17}$$

We can see that a solution can only be function of 4 parameters: $M, Re, Pr = \frac{c_p \mu}{k}, \gamma$, but we know that the geometry and the angle of attack α have a role by means of the boundary conditions. Then, we assume that the fluid is air ($\gamma = 1.4$) and that we can neglect heat effects (no influence of Pr , incompressible and so low speed flows). The non-dimensional lift, drag and moment are thus function of M, Re , geometry and α . We can define **lift**, **drag** and **moment coefficient** as (we forget about compressibility $\rightarrow M$, and Re effects are low for C_L and C_M):

$$\begin{aligned}
C_L(M, Re, geometry, \alpha) &= \frac{L}{\frac{1}{2} \rho_{ref} v_{ref}^2 S} \\
C_D(M, Re, geometry, \alpha) &= \frac{D}{\frac{1}{2} \rho_{ref} v_{ref}^2 S} \\
C_M(M, Re, geometry, \alpha) &= \frac{M}{\frac{1}{2} \rho_{ref} v_{ref}^2 S c}
\end{aligned} \tag{2.18}$$

where L, D, M are the **dimensional** forces, c the mean chord (S/b) and S a reference surface (3D wing \rightarrow total wing surface, 2D wing $\rightarrow S = c$). We can experimentally show that the lift increases mainly linearly with α and the drag force is caused by friction effects and pressure differences involving with α . This gives the following equations (lower case for 2D):

$$c_l = m(\alpha - \alpha_{L_0}) \quad c_d = c_{d_0} + k c_l^2 \tag{2.19}$$

where $m \approx 2\pi$ theoretically and 5.7 practically, k is a constant of order of magnitude 0.01.

2.4.2 Stall and critical angle of attack

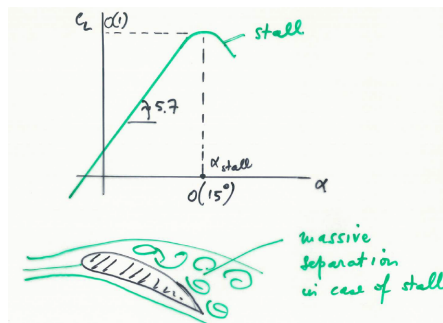


Figure 2.17

At a certain angle of attack ($\approx 15^\circ$), the lift suddenly drops. This is due to massive separation on the suction side (reverse pressure gradient too high) and happens at the **critical angle of attack**. This phenomenon is called **stall**. In the separated part, the pressure will no longer decrease and will form a pressure plateau.

We have to make the difference between leading-edge stall and trailing-edge stall. For **leading-edge stall**, the massive separation occurs suddenly near the LE resulting

in a strong and sudden drop of lift, when at maximum lift. This especially occurs to thin airfoils with cross-sections between 10 and 16% of the chord. For the **trailing-edge stall**, the point of separation gradually goes upstream with increasing angle of attack resulting in a more gradual drop of lift (more thick airfoils). The comparison is done on the right figure. We can also see a third type of stall called **thin airfoil stall** with the example of a flat plate.

In conclusion, the LE must be sufficiently rounded to have a good maximum lift. In fact the profile may nor be too

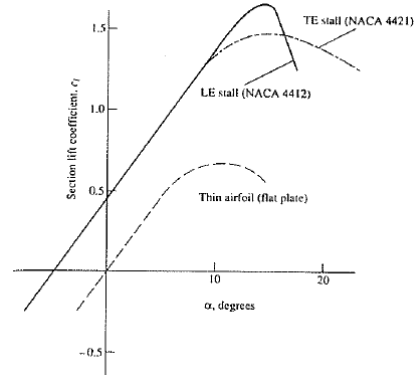


Figure 2.18

thick nor too thin. The figure on the left shows the influence of the thickness on the lift. We notice that the optimum thickness is situated around 12% of the chord. The maximum lift increases with RE, indeed higher the RE, higher is the ratio of speed versus viscosity. So we can better oppose to separation. Unlike the Re number, the roughness has great effects on the maximum lift. Finally, let's notice that the camber have also an effect on maximum lift, the best is a camber of 8 up to 10%.

2.4.3 Maximum lift, stalling speed, polar curve and glide ratio

From C_L in (2.18), we can deduce the lift:

$$L = C_L \frac{1}{2} \rho_{ref} v_{ref}^2 S. \quad (2.20)$$

The lift force must always at least be equal to the weight of the plane. This implies that for low speed (take-off and landing), the C_L must be large. This is accomplished with large α and slats or flaps. The minimum speed where the lift can still balance the weight (C_L maximum) is called **stall speed** and from (2.20) we find:

$$v_{stall} = \sqrt{\frac{W}{C_{L_{max}} \frac{1}{2} \rho_{ref} S}} \quad (2.21)$$

The curve that represents C_L in function of C_D is the **polar curve** of the wing. The ratio $\frac{C_L}{C_D}$ is the **glide ratio** or **finesse** and is like an efficiency parameter. The best parameter is obtained using the graph by calculating β such that:

$$\tan \beta = \left(\frac{C_L}{C_D} \right)_{max} \quad (2.22)$$

This point is important for the quality of the wing because if we plot the thrust, the lift, the drag and the weight of a plane describing a horizontal flight (Figure 2.21), the thrust is given by:

$$T = \frac{L}{\tan \beta} = \frac{W}{\tan \beta} \quad (2.23)$$

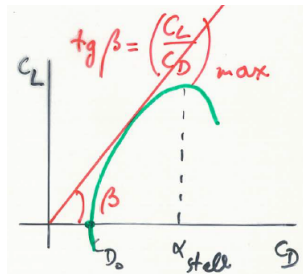


Figure 2.20

where we see that when $\tan \beta$ (so the glide ratio) increases, T decreases. Another interpretation can be given when we have no thrust (Figure 2.22). In this case the gliding ratio has to be adapted to travel the larger distance knowing that:

$$\frac{C_L}{C_D} = \frac{\text{distance travelled}}{\text{height loss}} \quad (2.24)$$

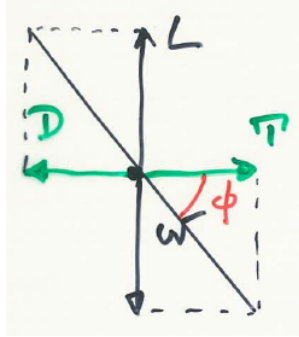


Figure 2.21

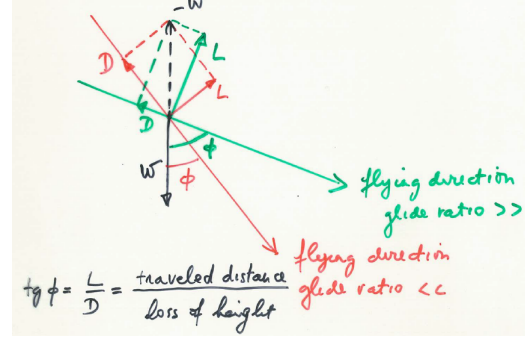


Figure 2.22

2.5 Methods to calculate flows around 2D airfoils

2.5.1 Conformal mapping

We will begin here with steady, inviscid irrotational flows. This gives for the mass conservation equation:

$$\frac{\partial \rho}{\partial t} + \nabla(\rho \vec{v}) = 0 \quad \Rightarrow \nabla \cdot \vec{v} = 0 = \partial_x u + \partial_y v \quad (2.25)$$

In the other hand, we have the assumption of irrotational flow:

$$\vec{\omega} = 0 \quad \Rightarrow \partial_x v - \partial_y u = 0. \quad (2.26)$$

Then we define the **complex potential function** w :

$$w = \phi + I\psi \quad (2.27)$$

where ϕ is the **potential function** (satisfies $w = 0$ by construction) such that:

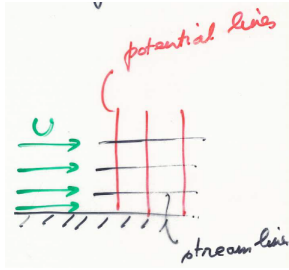
$$\begin{cases} u = \partial_x \phi \\ v = \partial_y \phi \end{cases} \quad \nabla \phi = \vec{v} = \partial_x \phi \vec{I}_x + \partial_y \phi \vec{I}_y \quad (2.28)$$

We must satisfy the mass conservation equation:

$$\nabla \cdot (\nabla \phi) = 0 \quad \Rightarrow \Delta \phi = 0 \quad (2.29)$$

coupled with boundary conditions, we can find a solution $\phi(x, y)$. The **stream function** satisfies the mass conservation by construction:

$$\begin{cases} u = \partial_y \psi \\ v = -\partial_x \psi \end{cases} \quad \Rightarrow \partial_x u + \partial_y v = 0 \Leftrightarrow \partial_x(\partial_y \psi) + \partial_y(-\partial_x \psi) = 0 \quad (2.30)$$



We still have to verify the $\omega = 0$ condition:

$$\partial_x v - \partial_y u = 0 \quad \Rightarrow \frac{\partial^2 \psi}{\partial x^2} + \frac{\partial^2 \psi}{\partial y^2} = 0 \quad \Delta \psi = 0 \quad (2.31)$$

A streamline and a potential line are perpendicular to each other:

$$\nabla \psi \cdot \nabla \phi = \partial_x \psi \partial_x \phi + \partial_y \psi \partial_y \phi = -vu + uv = 0. \quad (2.32)$$

Figure 2.23

Theory of analytical functions

Analytical means differentiable. This consist in defining a function $f(z)$ analytical such that:

$$w = f(z) \quad z, \omega \in \mathbb{C} \quad \Rightarrow w = \phi + i\psi \quad \begin{cases} z = x + iy \\ \phi = \phi(x, y) \in \mathbb{R} \\ \psi = \psi(x, y) \in \mathbb{R} \end{cases} \quad (2.33)$$

If this is differentiable everywhere, $\Delta\phi = \Delta\psi = 0$. We have a way to determine the complex velocity (velocity field):

$$\frac{dw}{dz} = \frac{df}{dz} = A + iB \quad A = \frac{\partial \phi}{\partial x} = -\frac{\partial \psi}{\partial y} = u \quad B = \frac{\partial \psi}{\partial x} = -\frac{\partial \phi}{\partial y} = -v \quad (2.34)$$

A property of this $f(z)$ is the superposition principle: $w_1 = f_1(z), w_2 = f_2(z)$ so $w_1 + w_2 = f_1(z) + f_2(z)$.

Uniform flow

This case corresponds to Figure ??:

$$w = Uz \quad \frac{dw}{dz} = U = u + iv \quad \Rightarrow u = U; v = 0 \quad (2.35)$$

Source / Sink

In this case, using the cylindrical coordinates, the complex potential is defined as (Λ being the volumetric flow):

$$w = \frac{\Lambda}{2\pi} \ln z = \frac{\Lambda}{2\pi} \ln(re^{i\theta}) = \frac{\Lambda}{2\pi} (\ln r + i\theta) \quad (2.36)$$

$$\Rightarrow \phi = \frac{\Lambda}{2\pi} \ln r, \psi = \frac{\Lambda}{2\pi} \theta.$$

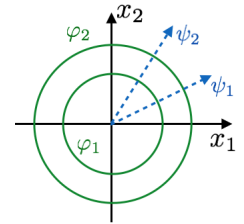


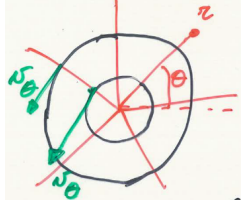
Figure 2.24

We see that complex lines corresponds to $r = cst$ so are circles and streamlines $\theta = cst$ are line of constant angle. $\oint \vec{v} d\vec{l} = 0$ as velocity is everywhere tangent to any circular contour. Let's compute the derivative for the velocity field:

$$\frac{dw}{dz} = \frac{\Lambda}{2\pi z} = \frac{\Lambda(x - iy)}{2\pi(x^2 + y^2)} = \frac{\Lambda}{2\pi r} (\cos \theta - i \sin \theta). \quad (2.37)$$

We see that the velocity decreases in $1/r$, this is due to the constant mass flow, so if the surface increases with r the velocity has to decrease to keep $\dot{m} = \rho v S$ constant.

Free vortex



We do the same as the other cases:

$$w = \frac{i\Gamma}{2\pi} \ln z = \frac{i\Gamma}{2\pi} \ln(re^{i\theta}) = \frac{i\Gamma}{2\pi} (\ln r + i\theta) = -\frac{\Gamma}{2\pi} \theta + \frac{i\Gamma}{2\pi} \ln r \quad (2.38)$$

$$\phi = -\frac{\Gamma}{2\pi} \theta, \psi = \frac{\Gamma}{2\pi} \ln r$$

Figure 2.25

We see that this is the inverse case of the previous one, streamlines are circles oriented in negative rotational motion around z-axis (z entering tin the sheet) so clockwise. We can compute the velocity field by deriving among z and we find that:

$$u = \frac{\Gamma \sin \theta}{2\pi r} \quad v = -\frac{\Gamma \cos \theta}{2\pi r} \quad (2.39)$$

Let's specify that $v_\theta = \frac{1}{r} \frac{\partial \phi}{\partial \theta} = -\frac{\Gamma}{2\pi r}$, and that we have a vortex singularity in the center because $\Gamma = 0.\infty$.

Flow around a cylinder

Let's make a combination of a uniform flow and a source + sink as shown on the figure. The combination gives:

$$w = Uz + \frac{\Lambda}{2\pi} \ln \frac{z+a}{z-a} = Uz + \frac{\Lambda}{2\pi} \ln \frac{1+a/z}{1-a/z}. \quad (2.40)$$

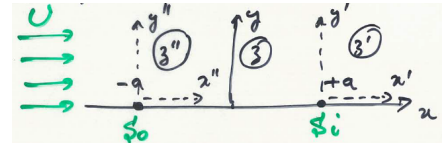


Figure 2.26

To have the flow around a cylinder we need to compute the limit $a \rightarrow 0$, and will need the Taylor expansion of \ln :

$$\ln \frac{1+\epsilon}{1-\epsilon} \approx 2\epsilon + o(\epsilon^2) \quad \Rightarrow \lim_{a \rightarrow 0} w = \lim_{a \rightarrow 0} \left[Uz + \frac{\Lambda}{2\pi} 2 \frac{a}{z} \right] \quad (2.41)$$

by defining $\mu = 2\Lambda a$ we find the **flow around a cylinder**:

$$w = Uz + \frac{\mu}{2\pi z}. \quad (2.42)$$

If we replace $z = x + iy$ to find ϕ and ψ we find:

$$\phi = Ux + \frac{\mu}{2\pi} \frac{x}{r^2} \quad \psi = Uy - \frac{\mu}{2\pi} \frac{y}{r^2}. \quad (2.43)$$

In this flow a closed streamline exists forming the so called **Rankine body** and which describes a cylinder in the case $a \rightarrow 0$. Indeed it is possible to find an exact solution for $\psi = 0$. This configuration has a symmetry according to x and y-axis when taking the center of the cylinder as origin. This implies that $\vec{F} = -\oint_{cyl} p d\vec{S} = 0$. This is the so called **paradox of d'Alembert** because we expect to find at least a drag force. A lift force can be find on the cylinder by adding a vortex. We conclude by saying that we can rewrite (2.42) as (R the radius of the cylinder):

$$w = U \left(z + \frac{R^2}{z} \right) \quad \text{with } R^2 = \frac{\mu}{2\pi U}. \quad (2.44)$$

Cylinder Joukowski transformation

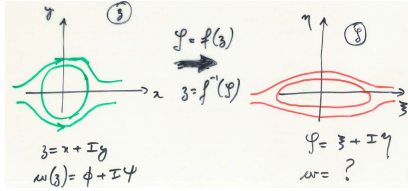


Figure 2.27

$$Z = z + \frac{R^2}{z} = Re^{i\theta} \frac{R^2}{Re^{i\theta}} = 2R \cos \theta \quad (2.45)$$

Indeed, as $\cos \theta \in [-1, 1]$ and the result is real, we have a flat plate between $-2R$ and $2R$ in the x -axis. The flow Z is directly found: $W(Z) = UZ$. The second example will be the application of the same transformation on a cylinder of this time radius $r > R$. In this case the circle becomes an ellipse:

$$Z = re^{i\theta} + \frac{R^2}{r^2} e^{-i\theta} = \left(r + \frac{R^2}{r} \right) \cos \theta + i \left(r - \frac{R^2}{r} \right) \sin \theta. \quad (2.46)$$

Let's also compute the velocity field using the chain rule:

$$\frac{dW}{dZ} = \frac{dw}{dZ} = \frac{dw}{dz} \frac{dz}{dZ} = \left(1 - \frac{r^2}{z^2} \right) \left(\frac{1}{1 - \frac{R^2}{z^2}} \right). \quad (2.47)$$

We see that the expression becomes infinite when $z^2 = R^2$. The reason is that the transformation is not analytical in these points so they must not be in the flow.

The examples are summarized in the figures below

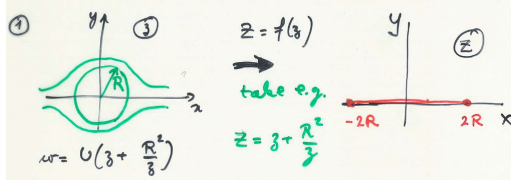


Figure 2.28

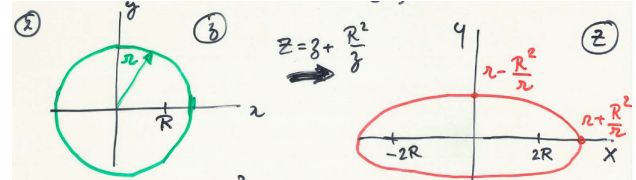


Figure 2.29

Now suppose that we place no longer the center of the cylinder at the origin, but on the real axis. The mapping of the cylinder now takes the shape of a **symmetrical wing profile**. We see that there are two remarkable points that are H and A corresponding to the points H_1 and A_1 of the black and red circles, our profile is in between them. Now to give camber we only have to move the center of the cylinder on the y-axis. Please reffer to figures below.

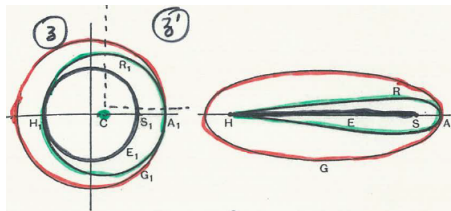


Figure 2.30

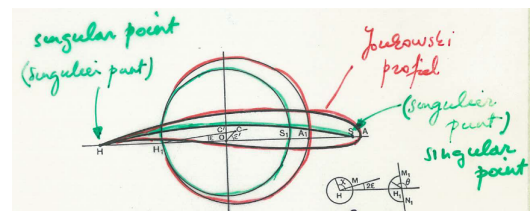


Figure 2.31

Note that for the green circle in first figure, the complex potential becomes:

$$w = U \left(z - z_c + \frac{r^2}{z - z_c} \right) \quad (2.48)$$

As last remark, let's remind that we had singularities in the second example. These points corresponds here to H_1 and S_1 . The mapping of H_1 is always H the trailing edge, the velocity is there infinitely large. This was the discussion we've previously done with the stagnation point that has to move on the trailing edge otherwise $v = \infty$ because of the sharp edge. We can solve this by adding a vortex. This methods gives a limited amount of airfoils.

2.5.2 Thin airfoil theory

We will suppose infinitely thin airfoil and small angle of attack, so that the airfoil is represented by the camber line. This means also small camber about 2-3% of the chord and $\alpha < 8\%$. We can try to retrieve the flow by superposition principle by using infinite number of elementary sources or elementary vortices. The potential function for the source and the elementary one are:

$$\phi = \frac{\Lambda}{2\pi} \ln r \quad d\phi = \frac{d\Lambda}{2\pi} \ln r \quad (2.49)$$

We then describe the source distribution by the source intensity $\lambda = \frac{d\Lambda}{ds}$ on a part ds of the wing so that the last equation becomes:

$$d\phi = \frac{\lambda}{2\pi} \ln r ds. \quad (2.50)$$

We will use the second method presented now which is using the vortices:

$$\phi = -\frac{\Gamma}{2\pi} \theta \quad \vec{v} = \nabla \phi = \underbrace{\frac{\partial \phi}{\partial r} \vec{l}_r}_{=v_r=0} + \underbrace{\frac{1}{r} \frac{\partial \phi}{\partial \theta} \vec{l}_\theta}_{=v_\theta} \Rightarrow v_\theta = -\frac{\Gamma}{2\pi r}. \quad (2.51)$$

In the same way as the other we can define a **vortex intensity** to characterize the vortex distribution on a part ds $\gamma = \frac{d\Gamma}{ds}$, the derivative of ϕ and the elementary velocity are then:

$$d\phi = -\frac{\gamma}{2\pi} \theta ds \quad dv_\theta = -\frac{\gamma ds}{2\pi r}. \quad (2.52)$$

The aim now is to make that infinitely thin airfoil a streamline, but which distribution of γ is needed? To compute this, we can assume because of superposition that the flow is a uniform flow \vec{U}_∞ . We also assume that we have an angle of attack α . Because of the vortices, we have a velocity perturbation \vec{v} such that the total velocity is:

$$\vec{V}_\infty = \vec{U}_\infty + \vec{v}. \quad (2.53)$$

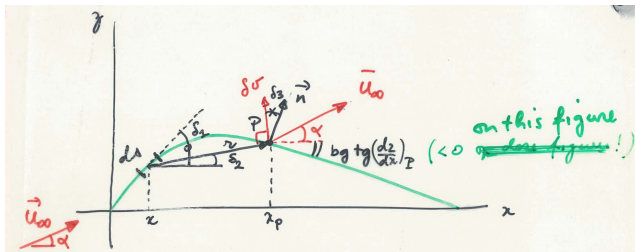


Figure 2.32

$- \arctan \left(\frac{dz}{dx} \right)_p$, the projection is (camber line: $z = f(x)$):

$$U_{\infty np} = U_\infty \sin \left[\alpha - \arctan \left(\frac{dz}{dx} \right)_P \right]. \quad (2.54)$$

We must now choose γ such that \vec{V} is tangential to the airfoil everywhere (we want the camber line to be a streamline). In other words, $\forall P$ the normal component of the velocity should be null $V_{np} = U_{\infty np} + v_{np} = 0$. Let's determine these components by projection. First, for $U_{\infty np}$ we can remark the sum of angle α and the camber line slope $\tan \beta = \left(-\frac{dz}{dx} \right)_P \Rightarrow \beta =$

Now for v_{np} , we consider an elementary vortex on a point x on the airfoil that creates an elementary perturbation δv_n on point P. This velocity direction is θ in a (r, θ) axis with origin at x, so perpendicular to r on the figure. If the angle with the normal is δ_3 , the projection will be:

$$\delta v_n = -\frac{\gamma(x)ds}{2\pi r} \cos \delta_3. \quad (2.55)$$

Now we have infinite number of contribution of the infinite vortices, as γ, r and δ_3 depends on position P , we have to integrate over the whole airfoil:

$$v_n = -\frac{1}{2\pi} \int_0^c \frac{\gamma(x)ds}{r} \cos \delta_3 \quad (2.56)$$

where c is the chord length. We can express both r and ds in function of x as:

$$r = \frac{x_P - x}{\cos \delta_2} \quad ds = \frac{dx}{\cos \delta_1} \quad (2.57)$$

which gives

$$v_n = -\frac{1}{2\pi} \int_0^c \frac{\gamma(x)dx}{x_P - x} \frac{\cos \delta_2}{\cos \delta_1} \cos \delta_3. \quad (2.58)$$

We are able to reconsider the condition (2.54) by replacing our results:

$$\frac{1}{2\pi} \int_0^c \frac{\gamma(x)dx}{x_P - x} \frac{\cos \delta_2}{\cos \delta_1} \cos \delta_3 = U_\infty \sin \left[\alpha - \arctan \left(\frac{dz}{dx} \right)_P \right]. \quad (2.59)$$

This is a relatively complicated equation, we can simplify it by **assuming a small camber** (in practice 2% of the chord), which allows to say that $\delta_1 \approx \delta_2 \approx \delta_3 \approx 0$ and $\arctan \left(\frac{dz}{dx} \right)_P = \left(\frac{dz}{dx} \right)_P$. By considering α small, $\sin \alpha \approx \alpha$:

$$\frac{1}{2\pi} \int_0^c \frac{\gamma(x)dx}{x_P - x} = U_\infty \left[\alpha - \left(\frac{dz}{dx} \right)_P \right]. \quad (2.60)$$

We will introduce a new variable θ and not anymore describe the system using x by considering $x = \frac{1}{2}c(1 - \cos \theta)$ and $dx = \frac{1}{2}c \sin \theta d\theta$:

$$\frac{1}{2\pi} \int_0^\pi \frac{\gamma(\theta) \sin \theta d\theta}{\cos \theta - \cos \theta_P} = U_\infty \left[\alpha - \left(\frac{dz}{dx} \right)_P \right]. \quad (2.61)$$

This is a quite difficult equation, so let's complicate it even more by expressing $\gamma(\theta)$ in series:

$$\gamma(\theta) = 2U_\infty \left(A_0 \coth \frac{\theta}{2} + \sum_{n=1}^{\infty} A_n \sin(n\theta) \right). \quad (2.62)$$

This is in fact a solution of the last equation but we will not demonstrate it. Notice simply that this respects the Kutta condition that states that there is no vortex allowed on the trailing edge. Indeed for $\gamma(\pi) = 0$ which means no contribution by vortex. We can also state that at the leading edge, the stagnation point is in the pressure side at the front. Indeed, for $\theta = 0$, $\coth \theta = \infty = \gamma(\pi)$ which means that we have a singularity at the TE and that the velocity is infinite due to the turning on the LE.

Now we can replace this definition on the previous equation, knowing that $\coth(\theta/2) \sin \theta = 1 + \cos \theta$ and renoting $\theta_P = \theta'$, we get:

$$\frac{1}{2\pi} \int_0^\pi \frac{\gamma(\theta) \sin \theta d\theta}{\cos \theta - \cos \theta_P} = \frac{U_\infty}{\pi} \left[\int_0^\pi \frac{A_0(1 + \cos \theta) d\theta}{\cos \theta - \cos \theta'} + \sum_n A_n \int_0^\pi \frac{\sin(n\theta) \sin \theta d\theta}{\cos \theta - \cos \theta'} \right] \quad (2.63)$$

By using the equality here and the **Glauert integral**:

$$\sin(n\theta) \sin \theta = -\frac{1}{2} [\cos[(n+1)\theta] - \cos[(n-1)\theta]] \quad \int_0^\pi \frac{\cos(n\theta) d\theta}{\cos \theta - \cos \theta'} = \pi \frac{\sin(n\theta')}{\sin \theta'} \quad (2.64)$$

The integral becomes:

$$\frac{U_\infty}{\pi} \left[A_0 \cdot 0 + A_0 \cdot \pi - \frac{\pi}{2} \sum_n A_n \frac{\sin[(n+1)\theta'] - \sin[(n-1)\theta']}{\sin \theta'} \right] = U_\infty \left[A_0 - \sum_n A_n \cos(n\theta') \right] \quad (2.65)$$

where we used the simpson equation. The (2.61) becomes:

$$A_0 - \sum_n A_n \cos(n\theta') = \alpha - \left(\frac{dz}{dx} \right)' \quad (2.66)$$

This equation must be valid $\forall P$ on the airfoil. To find the coefficients A_i , let's integrate first this for $0 \leq \theta' \leq \pi$ in order to compute A_0 :

$$A_0 \pi - \sum_n A_n \overbrace{\int_0^\pi \cos(n\theta') d\theta'} = \alpha \pi - \int_0^\pi \frac{dz}{dx} d\theta \quad \Rightarrow A_0 = \alpha - \frac{1}{\pi} \int_0^\pi \frac{dz}{dx} d\theta. \quad (2.67)$$

For the A_n , we multiply the same equation by $\cos(m\theta')$ before integrating (we will drop the '). Let's see that $\int_0^\pi \cos(n\theta) \cos(m\theta) d\theta = 0$ if $m \neq n$ and $= \pi/2$ if $n = m$. We finally get:

$$A_n = \frac{2}{\pi} \int_0^\pi \frac{dz}{dx} \cos(m\theta) d\theta. \quad (2.68)$$

We can note that for A_n only the camber plays a role, the angle of attack does not appear. Only A_0 is influenced by α . We are now able to compute any vorticity distribution $\gamma(\theta)$, for example for a flat plate $A_n = 0$ and $A_0 = \alpha$.

Calculation of the total circulation

To get Γ we only have to compute the integral over the whole airfoil:

$$\begin{aligned} \Gamma &= \int_0^c \gamma(x) dx = \frac{1}{2} c \int_0^c \gamma(\theta) \sin \theta d\theta \\ &= \frac{1}{2} c \left[2U_\infty \int_0^\pi A_0(1 + \cos \theta) d\theta + 2U_\infty \sum_{n=1}^{\infty} \int_0^\pi A_n \sin(n\theta) \sin \theta d\theta \right] \\ &= U_\infty c \left[A_0 \pi + 2U_\infty + \int_0^\pi \sin^2(\theta) d\theta - \frac{1}{2} \sum_{n=2}^{\infty} \int_0^\pi A_n \cos[(n+1)\theta] - \cos[(n-1)\theta] d\theta \right] \\ &= U_\infty c [A_0 \pi + A_1 \pi / 2]. \end{aligned} \quad (2.69)$$

We see that the circulation only depends on two coefficients.

Calculation of the lift coefficient

We can now compute the lift using the kutta formula $L = \rho_\infty U_\infty \Gamma$. We are interested in the c_l and not the lift itself. In 2D we have to divide by the chord so:

$$c_l = \frac{L}{\frac{1}{2} \rho_\infty U_\infty^2 C} = \frac{2\Gamma}{U_\infty c} = \pi(2A_0 + A_1) \quad (2.70)$$

We can now replace by definition of the coefficients:

$$c_l = 2\pi \left(\alpha - \underbrace{\frac{1}{\pi} \int_0^\pi \frac{dz}{dx} (1 - \cos \theta) d\theta}_{\alpha_0} \right) = 2\pi(\alpha - \alpha_0) \quad (2.71)$$

where α_0 is the **zero lift angle of attack**. We see that we have a linear relation with respect to α . We have the theoretical model the same for every profile, only α_0 changes with the profile. Remark that the lift is also the integral of the pressure on the lower and upper side:

$$L = \int_0^c (p_l - p_u) dx = \rho_\infty U_\infty \int_0^c \gamma dx \quad \Rightarrow p_l - p_u = \rho_\infty U_\infty \gamma(x). \quad (2.72)$$

Calculation of the momentum at the leading edge



Figure 2.33

The contribution of the elementary parts of the airfoil gives:

$$\begin{aligned} dM_{LE} &= -(\Delta p dx)x \\ \Rightarrow M_{LE} &= - \int_0^c \Delta p x dx = -\rho_\infty U_\infty \int_0^c \gamma x dx \end{aligned} \quad (2.73)$$

After some manipulations (not detailed):

$$c_{m_{LE}} = \frac{M_{LE}}{\frac{1}{2} \rho_\infty U_\infty^2 c^2} = -\frac{\pi}{4}(2A_0 + 2A_1 - A_2) = -\frac{1}{4}c_l - \frac{\pi}{4}(A_1 - A_2) \quad (2.74)$$

where we used (2.70) for the last expression. This is of the same shape than (2.11) with negative k.

The aerodynamic center



Figure 2.34

The moment on the LE is related to the moment anywhere:

$$M_{LE} = M_{ac} - x_{ac}L \quad \Rightarrow c_{m_{LE}} = c_{m_{ac}} - \frac{x_{ac}}{c}c_l \quad (2.75)$$

By using the last result of the previous section, we get:

$$c_{m_{ac}} = \left(\frac{x_{ac}}{c} - \frac{1}{4} \right) c_l - \frac{\pi}{4}(A_1 - A_2). \quad (2.76)$$

We see that, for this relation to be independent of the angle of attack, we must have $x_{ac} = \frac{c}{4}$ so that:

$$c_{m_{ac}} = \frac{\pi}{4}(A_2 - A_1). \quad (2.77)$$

Remark that for symmetrical wings $\frac{dz}{dx} = 0 \Rightarrow A_1 = A_2 = 0 \Rightarrow c_{m_{ac}} = 0$.

Calculation of center of pressure

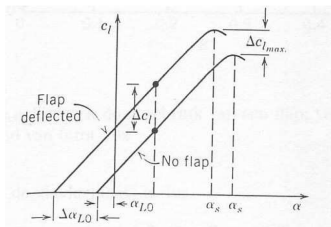
The formula used in the previous section is valid, we replace ac by cp, and since the moment should be null at this point:

$$c_{m_{cp}} = c_{m_{LE}} + \frac{x_{cp}}{c} c_l = 0 \quad \Rightarrow \quad \frac{x_{cp}}{c} = \frac{1}{4} + \frac{\frac{\pi}{4}(A_1 - A_2)}{c_l} = \frac{1}{4} - \frac{c_{m_{ac}}}{c_l}. \quad (2.78)$$

Some remarks:

- the center of pressure is not fixed and varies with the lift
- at 0 lift, $x_{cp} \rightarrow \infty$ (for symmetric wing $x_{cp} = x_{ac} = c/4$ fixed)
- cp always downstream to ac because $c_{m_{ac}} < 0$.

Effect of flaps



According to the definition of the zero lift angle in (2.71), the effect of the shape becomes greater when $\theta \approx 180^\circ$ (trailing edge). By making the zero lift angle more negative we can produce more lift before the critical angle of attack that decreases a bit.

Figure 2.35

The effect is evaluated by taking a flat plate as camber line with a deflection near the TE, starting at E% of the chord and slope η . E in function of θ_E is:

$$E = \frac{1}{2}(1 + \cos \theta_E). \quad (2.79)$$

In this case, A_0 and A_n can be rewritten as:

$$\begin{aligned} A_0 &= \alpha - \frac{1}{\pi} \int_0^\pi \frac{dz}{dx} d\theta \approx \alpha - \frac{\eta}{\pi}(\pi - \theta_E) \\ A_n &= \frac{2}{\pi} \int_0^\pi \frac{dz}{dx} \cos(n\theta) d\theta \approx -\frac{2\eta}{\pi n} \sin(n\theta_E) \end{aligned} \quad (2.80)$$

such that the lift coefficient becomes:

$$c_l = \pi(2A_0 + A_1) = \underbrace{2\pi\alpha}_{\text{without flaps}} - \underbrace{-2\eta(\pi - \theta_E + \sin \theta)}_{\Delta c_l > 0 \text{ since } \eta < 0}. \quad (2.81)$$

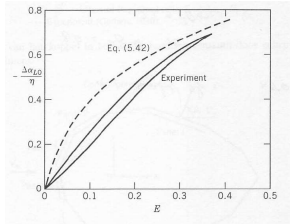
This seems to be like $c_l = 2\pi(\alpha - \alpha_0)$ allowing the definition for the zero lift angle:

$$\alpha_0 = \frac{\eta}{\pi}(\pi - \theta_E + \sin \theta) \quad (2.82)$$

which indicates an increase (decrease since $\eta < 0$) of α_0 since it is null for the flat plate. For the moment at the ac (2.77)

$$\Delta c_{m_{ac}} = \frac{\eta}{2} \sin \theta_E (1 - \cos \theta_E) \quad (2.83)$$

which also indicates a decrease in the momentum which is 0 for the symmetric wing.



Here is plotted the the modification of α_0 by the flaps. The theory is quite good except for small E (near the TL). This is due to the fact that the flap is immersed into the boundary layer in this region.

Figure 2.37

2.5.3 Numerical methods: source panel and vortex panel

Source panel

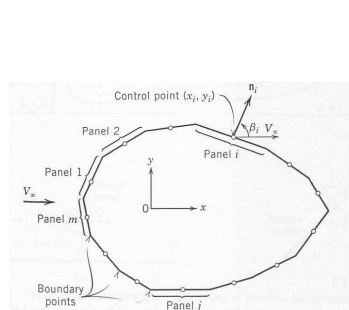


Figure 2.38

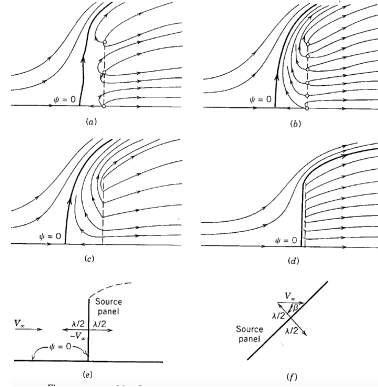


Figure 2.39

The method consists in subdividing the geometry into panels that each contains a source with source intensity $\lambda_j = \frac{d\Lambda_j}{ds_j}$, where $d\Lambda_j$ is the elementary volumetric flow rate associated to the part ds_j . The second figure illustrates the panel concept. We can see the flow obtained by placing sources on a vertical line. From a to d the number of sources increases but the total flow remains the same (d reduced flow rate).

Using an infinite number of sources and a constant λ , we obtain a panel in e. Remark that the velocity is perpendicular to the plate in that case.

Next we have to write the potential function and express that the flow should be tangential to the plate. Remark that since there is no vortex the lift is null.

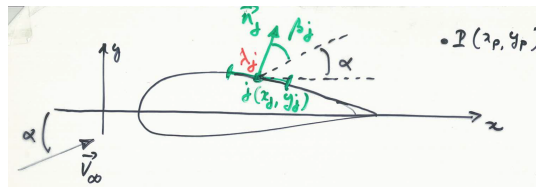


Figure 2.40

Consider the airfoil here and let's write the potential function for the uniform flow at point P:

$$\phi_{uP} = U_\infty \cos \alpha x + U_\infty \sin \alpha y \quad (2.84)$$

On the other hand, the source distribution on panel j also generates a potential function:

$$\phi_{jP} = \int_{\text{panel } j} \frac{\lambda_j}{2\pi} \ln(r_{jP}) ds_j \quad r_{jP} = \sqrt{(x_P - x_j)^2 + (y_P - y_j)^2}. \quad (2.85)$$

The total potential is the sum of all that and all the panels j. The condition for the flow to be tangential to panel i is $\frac{\partial \phi}{\partial n_j} = 0$. This applied to our total potential gives (P is the control point of the panel i):

$$U_\infty \cos \beta_i + \sum_j \frac{\lambda_j}{2\pi} \int_{\text{panel } j} \frac{\partial}{\partial n_i} (\ln(r_{ji})) ds_j = 0, \quad (2.86)$$

where λ_j is assumed to be constant on panel j . The integral regroups the effect of panel j on the normal component of the velocity on panel i , this is only function of the geometry! Note that even if the effect of panel i on its own component leads to $r_{ji} = r_{ii} = 0$ (singular integral), one can show that:

$$\int_{\text{panel } i} \frac{\partial}{\partial n_i} (\ln(r_{ii})) ds_i = \pi, \quad (2.87)$$

so that the contribution of the panel i is reduced to $\lambda/2$, reducing the general equation to:

$$U_\infty \cos \beta_i + \frac{\lambda}{2} + \sum_{j \neq i} \frac{\lambda_j}{2\pi} \int_{\text{panel } j} \frac{\partial}{\partial n_i} (\ln(r_{ji})) ds_j = 0. \quad (2.88)$$

Since this is a system of N equations in N unknowns (N panel), we are able to find every λ_i . Using again the potential function, we are able to get now the tangential velocity at panel i :

$$v_{ti} = \frac{\partial \phi}{\partial s_i} = U_\infty \sin \beta_i + \sum_j \frac{\lambda_j}{2\pi} \int_{\text{panel } j} \frac{\partial}{\partial s_i} (\ln(r_{ji})) ds_j. \quad (2.89)$$

Since a panel i only generates a normal velocity, it has no effect on its own tangential velocity, we can show that:

$$\int_{\text{panel } i} \frac{\partial}{\partial s_i} (\ln(r_{ii})) ds_i = 0 \quad (2.90)$$

simplifying the previous equation by getting a $\sum_{j \neq i}$. It is then possible to retrieve the pressure distribution along the geometry by applying Bernoulli:

$$c_{pi} = 1 - \left(\frac{v_{ti}}{U_\infty} \right) \quad (2.91)$$

Vortex panel



Figure 2.41

This method is similar to the previous one, and since we discussed the thin airfoil theory, we can directly use the definition of the potential function:

$$U_\infty \cos \alpha x + U_\infty \sin \alpha y - \sum_j \frac{\gamma_j}{2\pi} \int_{\text{panel } j} \theta_{jP} ds_j. \quad (2.92)$$

The assumptions made on the previous section are reused here (first order method: intensity constant). The angle θ_{jP} is the θ -value describing the position of P in a coordinate system centered in the control point of panel j :

$$\tan \theta_{jP} = \frac{y_P - y_j}{x_P - x_j}. \quad (2.93)$$

As previously, we compute the vorticity distribution by expressing the condition of null normal potential on the panel:

$$\frac{\partial \phi}{\partial n_i} = U_\infty \cos \beta_i - \sum_{j \neq i} \frac{\gamma_j}{2\pi} \int_{\text{panel } j} \frac{\partial}{\partial n_i} (\theta_{ji}) ds_j = 0. \quad (2.94)$$

Similarly we get a system of N equation of N unknowns. But we have a circulation in this case and we have to satisfy the Kutta condition which states that the vortex distribution on the trailing must be 0. Referring to the figure, the Kutta condition can be approximated as:

$$\gamma_i = -\gamma_{i-1}. \quad (2.95)$$

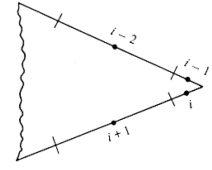


Figure 2.42

With this, we get an overdetermined system of $N+1$ equations for N unknowns so we can drop one of the panel equation. Once these are solved, we can get the tangential velocity distribution on the body:

$$v_{ti} = \frac{\partial \phi}{\partial s_i} = U_\infty \sin \beta_i - \sum_j \frac{\gamma_j}{2\pi} \int_{\text{panel } j} \frac{\partial}{\partial s_i} (\theta_{ji}) ds_j = U_\infty \sin \beta_i + \gamma_i. \quad (2.96)$$

The last γ can be understood intuitively. If we remind the previous method, we had a perpendicular velocity on both side of the source panel of intensity $\lambda/2$. Analogously, the vorticities produce a velocity this time tangential to the panel, in opposite direction on both side of the panel, with size $\gamma/2$. The velocity increases with γ when moving from one side to the other. Because of the contribution of the other vorticities, there is no flow in the inner part of the panel, but the jump of velocity remains, causing the velocity on the outer side to become γ .

The lift is found by using Kutta-Joukowski formula:

$$\Gamma = \sum_j \gamma_j s_j \Rightarrow L = \rho_\infty U_\infty \Gamma. \quad (2.97)$$

Remark: a second order method can be used, choosing the control points on the corner of the panel and postulating a linear variation of the intensity along the panel. In this case the Kutta condition reduces to:

$$\gamma_1 = 0. \quad (2.98)$$

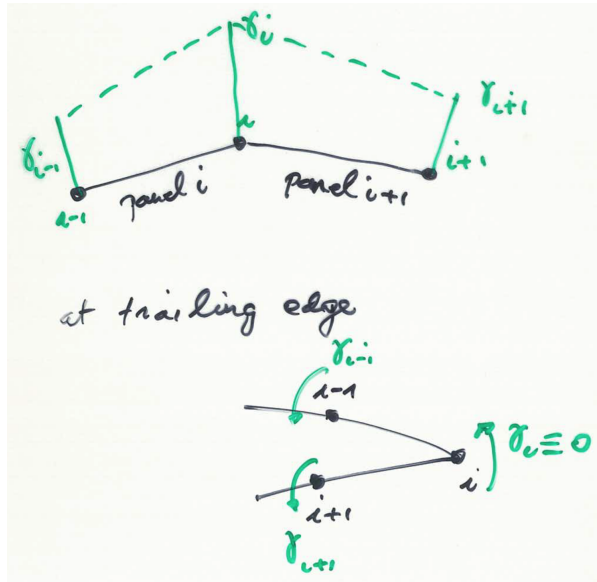


Figure 2.43

Chapter 3

The 3D wing

Before the main subject, here is some precision about the terminology:

- b is the **span**
- $c = \frac{S}{b}$ is the **mean chord**
- $s = \frac{b}{2}$ is the **semi span**
- $AR = \frac{b}{c} = \frac{b^2}{S}$ is the **aspect ratio**
- we speak about a **tapered wing** if $c_{tip} < c_{root}$ and the taper ratio is $\frac{c_{tip}}{c_{root}}$
- we speak about a **swept wing** when the leading edge and/or the trailing edge line is not \perp to the flow.

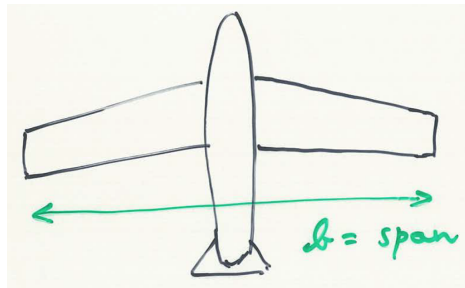


Figure 3.1

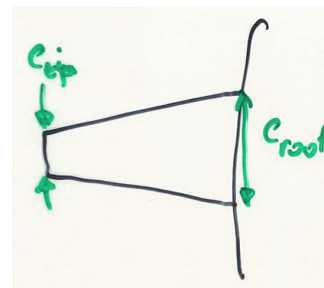


Figure 3.2

3.1 The downwash effect and the induced drag

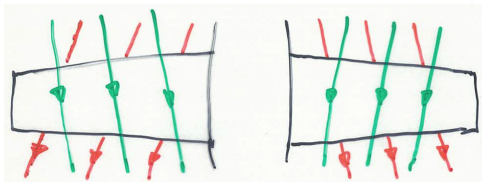


Figure 3.3

The 3D wing changes from the 2D case, because we have a finite span. As we know, we have a suction side and a pressure side. The thing is that because of the tip, the pressure on both sides must be equal at the end of the span. This means that the pressure on the upper side must increase when going to the tip, and decrease on the lower side. This creates a pressure gradient between the root and the tip. This gradient will push the streamlines on the upper side towards the fuselage and towards the tip on the lower side.

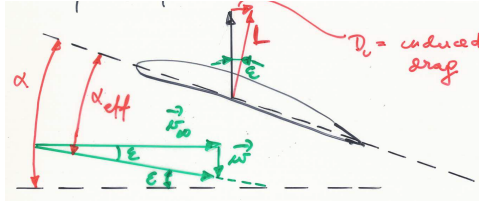


Figure 3.4



Figure 3.5

If we look to the trailing edge from a position downstream to the wing, this discontinuity in velocity induces an infinite series of infinitely small vortices, clockwise on the left and anti clockwise on the right wing (Figure 3.4). In practice these vortices are unstable and result into 2 discrete vortices at the tip, the so called **wing-tip vortices or trailing vortices** (Figure 3.5).



These vortices have an effect on the neighboring flow, they induce a **downward velocity component, the downwash \bar{w}** . This component superposes on the incoming flow and changes the angle of attack. Figure 3.6 shows that the resulting angle is:

Figure 3.6

$$\alpha_{eff} = \alpha - \epsilon \quad (3.1)$$

where ϵ is the induced angle of attack. The decrease of α means a decrease in lift. Indeed, initially the flow being horizontal, the perpendicular lift was vertical. The new lift is perpendicular to the resulting flow direction, describing now an **induced drag**:

$$D_i = L \sin \alpha_i \approx L \alpha_i \quad \text{with} \quad \alpha_i = \frac{C_L}{\pi e AR} \quad (3.2)$$

where e is the **span efficiency factor or Oswald's efficiency factor** $0.85 < e < 1$. If we introduce this in the definition of the induced drag, we get the Drag coefficient:

$$C_{D_i} = \frac{C_L^2}{\pi e AR}. \quad (3.3)$$

The theoretical lift curve can be obtained based on the 2D wing as Figure 3.7. We can see that the 3D wing lift for a certain α corresponds to the 2D lift for the effective angle of attack $\alpha - \epsilon$. The induced angle of attack decreases with lift, at α_0 the two curves are on the same point. Algebraically the 2D and 3D curves can be noted:

$$c_l = m(\alpha - \alpha_0), \quad C_L = m(\alpha - \epsilon - \alpha_0) = m^*(\alpha - \alpha_0) \quad (3.4)$$

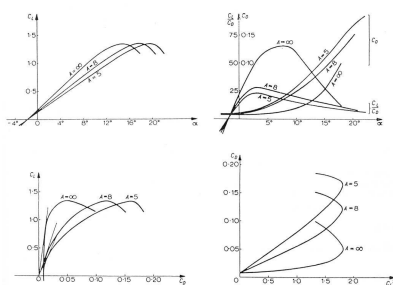
where m^* is the slope of the 3D lift. We can isolate this and find that:

$$m^* = m \left(1 - \frac{\epsilon}{\alpha - \alpha_0} \right) = \frac{m}{1 + \frac{m}{\pi e AR}} \quad (3.5)$$

where we used the definition (3.2) and (3.4) for the last result. We see that the slope is independent from α . The total drag is the sum of the profile drag and the induced one:

$$C_D = C_{D_0} + k C_L^2 + C_{D_i} = C_{D_0} + C_L^2 \left(k + \frac{1}{\pi e AR} \right) \quad (3.6)$$

where k is generally small compared to the other.



With these formulas we can plot the characteristics in 3D. We can note that the maximum lift does not change so more, but there is a strong decrease in the maximum glide ratio, C_D increases with C_L so α . Finally we note an increase of the stall angle but in practice this is not as large as predicted. This means also that the maximum lift decreases slightly with decreasing AR. No significant difference for the moment.

Figure 3.8

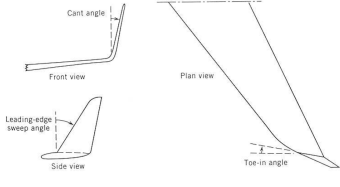


Figure 3.9

3.1.1 Variation of the drag during the flight

We found the drag coefficient on the wing but we have also the drag coming from the fuselage, etc. These part does not contribute in lift so they are called **parasite drag**. Let's compute the total drag using the coefficient definition:

$$D = C_D \frac{1}{2} \rho_\infty v_\infty^2 S = C_{D_0} \frac{1}{2} \rho_\infty v_\infty^2 S + \left(k + \frac{1}{\pi e A R} \right) \frac{L^2}{(\frac{1}{2} \rho_\infty v_\infty^2 S)^2} \frac{1}{2} \rho_\infty v_\infty^2 S \\ = k_1 v_\infty^2 + k_2 v_\infty^2. \quad (3.7)$$

If the plane is in stationary flight, the lift is equal to the weight W of the plane. One can write, introducing a and b bigger than the previous coefficients in order to take into account the drag furnished by the whole plane:

$$k_1 = C_{D_0} \frac{1}{2} \rho_\infty S = a \frac{1}{2} \rho_\infty S \\ k_2 = \left(k + \frac{1}{\pi e A R} \right) \frac{W^2}{\frac{1}{2} \rho_\infty S} = b \frac{W^2}{\frac{1}{2} \rho_\infty S} \quad (3.8)$$

where the terms k_1 and k_2 represent the profile drag and the induced drag. An important conclusion is that the profile drag increases with the square of velocity while the induced drag does the contrary. We can find a point of minimum drag by canceling D in (3.7):

$$v_{min}^4 = \frac{k_2}{k_1} \quad \Rightarrow D_{min} = 2\sqrt{k_1 k_2} = 2W\sqrt{ab}. \quad (3.9)$$

This is only dependent of the weight. This minimum velocity gives the lower limit of the region where the plane is well controllable. Indeed, for a small decrease, we increase the drag that will decrease the velocity and so on. This is an unstable situation. Note that the minimal velocity is higher than the stall velocity. Remark that the dashed curves on the graph take into account the separation occurring due to the drag. We find two solution, this is logical as in c_l we can have the same lift with two α .

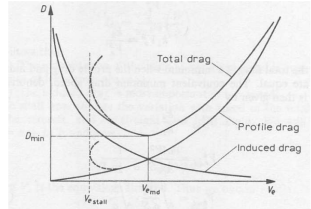


Figure 3.10

3.2 Prandtl lifting line theory

3.2.1 Introduction : vortex lines and law of Biot-Savart

Vortex lines and the Helmholtz theorems

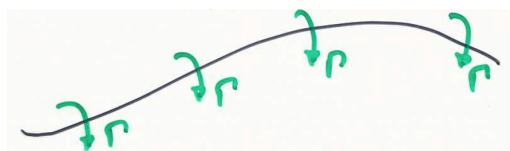


Figure 3.11

The seen free vortex is characterized by circular streamlines around a certain point P . In this point the vorticity is concentrated such that the circulation around the contours that don't contain the point are null. If we consider several planes above each other containing a 2D free vortex, the point P

form a line called **vortex line or vortex filament**. The circulation on each point of that line have the same circulation.

Helmholtz theorems

- Along a vortex line, the circulation must be constant.
- A vortex line cannot finish in the flow but must continue to the edges of the flow or form a closed contour.

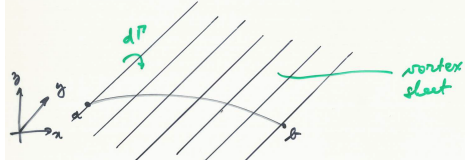


Figure 3.12

This line can be a random line with bending. Now if one places an infinite number of vortex lines besides each other, we get a **vortex sheet**. For the total circulation to be finite, the circulations must be infinitely small, but can vary from one line to the other. The circulation of the vortex sheet is calculated as:

$$\Gamma = \int_a^b d\Gamma = \gamma ds \quad \text{and} \quad \Delta v_t = \gamma \quad (3.10)$$

the normal component of the velocity is continuous while the tangential one varies as in the last equation.

Law of Biot-Savart

This law gives the induced velocity in a certain point P cause by an elementary piece $d\vec{l}$ of the filament:

Law of Biot-Savart

$$d\vec{v} = \frac{\Gamma}{4\pi} \frac{d\vec{l} \times r}{|r|^3} \quad (3.11)$$

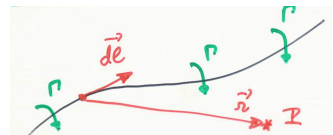


Figure 3.13

With analogy to electrical wire where we have a current intensity that induces a magnetic field on point P: $d\vec{B} = \frac{\mu I}{4\pi} \frac{d\vec{l} \times r}{|r|^3}$.

Application of Biot-Savart to a vortex filament

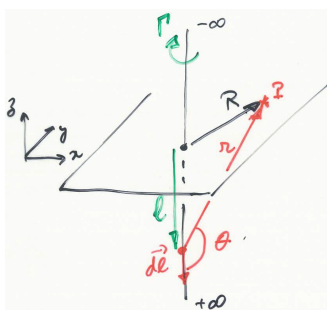


Figure 3.14

The law tells us that at point P:

$$\vec{v} = \frac{\Gamma}{4\pi} \int_{-\infty}^{+\infty} \frac{d\vec{l} \times r}{|r|^3}. \quad (3.12)$$

Looking to the figure, we see that $d\vec{l} \times \vec{r} = R dl \vec{1}_n$ defined on the figure. So $\vec{v} = v \vec{1}_n$. Let's define the length l beginning from the piercing point on the surface until the $d\vec{l}$. We can graphically see that:

$$l = -R \coth \theta \Rightarrow dl = \frac{R}{\sin^2 \theta} d\theta, \quad r = \frac{R}{\sin \theta} \quad (3.13)$$

Replacing all this we get:

$$v = \frac{\Gamma}{4\pi} \int_0^\pi \frac{R^2}{\sin^2 \theta} \frac{\sin^3 \theta}{R^3} d\theta \Rightarrow v = \frac{\Gamma}{2\pi R}. \quad (3.14)$$

This is the velocity distribution of the 2D free vortex.

3.2.2 Prandtl lifting line formula

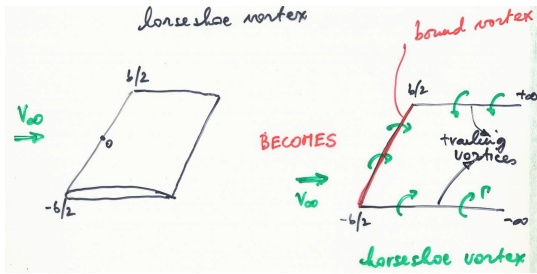


Figure 3.15

The idea is to represent the 3D wing by means of vortex filaments. On the figure we have the **horseshoe vortex** where the x direction continues to infinity to satisfy the Helmholtz condition and the y direction extends from $-b/2$ to $b/2$ and represents the two wings. This last is the bound vortex and the one in x direction represents the tip vortices. The problem with the representation is that we have a constant circulation while we have seen that the lift decreases when going to the tips.

Let's try to compute the downwash velocity on a point from the bound vortex. The law of Biot-Savart has 3 contributions:

$$\vec{v} = \int_{-\infty}^{-b/2} \dots + \int_{-b/2}^{b/2} \dots + \int_{b/2}^{\infty} \dots . \quad (3.15)$$

The second integral vanishes as dl and r are parallel, the two others were computed at the previous section. Pay attention that we have to take half the contribution as the integral is not $-\infty, +\infty$:

$$\vec{v}(y) = \left(\frac{\Gamma}{4\pi R} + \frac{\Gamma}{4\pi R^*} \right) \vec{l}_n \quad (3.16)$$

We can see that the velocity is infinity at the tips and minimum at the middle. This is clearly not the reality.

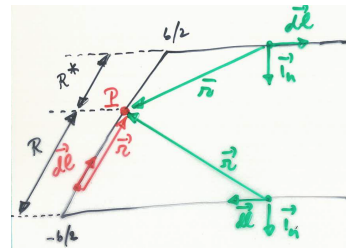


Figure 3.16

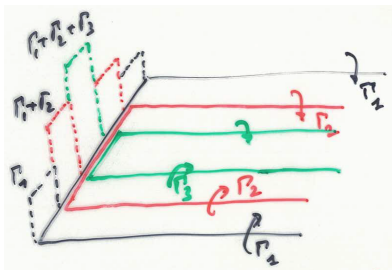


Figure 3.17

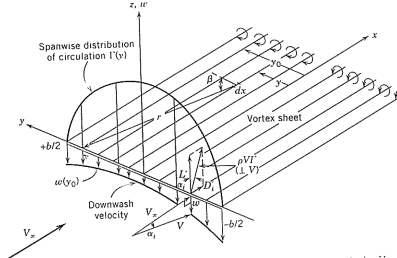


Figure 3.18

The solution is to superpose the horseshoes with bound vortices with different length. ?? shows how the superposition affects the circulation on the wing. If now we let tend the number of superimposed horseshoe vortices to infinity, we will get a vortex sheet as represented on Figure 3.18. The continuously varying circulation on the wing is no longer constant and this corresponds better with the reality.

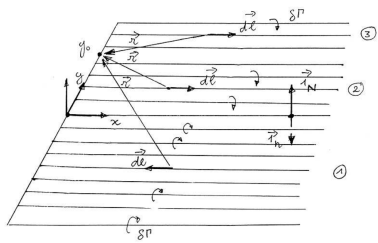


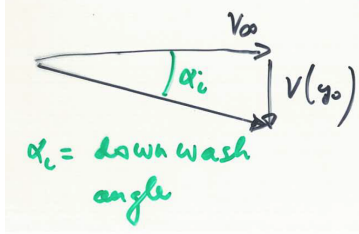
Figure 3.19

Consider this figure, we will try to compute the downwash velocity by considering a large but finite number of vortices of circulation $d\Gamma$ for each. We have 3 regions to consider with our basic formula:

- $y < 0$: $d\vec{v}(y_0) = \frac{d\Gamma}{4\pi(y_0-y)} \vec{l}_n$
- $0 < y < y_0$: $d\vec{v}(y_0) = \frac{d\Gamma}{4\pi(y_0-y)} \vec{l}_N = \frac{-d\Gamma}{4\pi(y_0-y)} \vec{l}_n$
- $y_0 < y$: $d\vec{v}(y_0) = \frac{d\Gamma}{4\pi(y-y_0)} \vec{l}_n = \frac{-d\Gamma}{4\pi(y-y_0)} \vec{l}_n$

We can see that the three formulas are the same if we take $\Gamma < 0$ for $y > 0$. We can so write the total contribution and its extension to the infinite number of lines:

$$\vec{v} = \left[\sum \frac{d\Gamma}{4\pi(y_0 - y)} \right] = \left[\int_{-b/2}^{b/2} \frac{d\Gamma}{4\pi(y_0 - y)} \right] \quad (3.17)$$



The induced angle of attack is then given by:

$$\tan \alpha_i \approx \alpha_i = \frac{v(y_0)}{v_\infty} = \frac{1}{4\pi v_\infty} \int_{-b/2}^{b/2} \frac{d\Gamma}{y_0 - y}. \quad (3.18)$$

Now let's denote $\alpha_{eff} = \alpha - \epsilon$. We know that the theory says $c_l = 2\pi(\alpha_{eff}(y_0) - \alpha_0(y_0))$, and using the definition of c_l and the Kutta-Jukowski for $L(y_0)$ we get:

Figure 3.20

$$\begin{aligned} c_l &= \frac{L(y_0)}{\frac{1}{2}\rho_\infty v_\infty^2 c(y_0)} = \frac{\rho_\infty v_\infty \Gamma(y_0)}{\frac{1}{2}\rho_\infty v_\infty^2 c(y_0)} = \frac{\Gamma(y_0)}{\frac{1}{2}v_\infty^2 c(y_0)} \\ \Rightarrow \alpha_{eff} &= \frac{\Gamma(y_0)}{\pi v_\infty c(y_0)} + \alpha_0(y_0) \end{aligned} \quad (3.19)$$

Combining all the result, we can compute the α :

Fundamental equation of Prandtl's lifting line theory

$$\alpha(y_0) = \frac{\Gamma(y_0)}{\pi v_\infty c(y_0)} + \alpha_0(y_0) + \frac{1}{4\pi v_\infty} \int_{-b/2}^{b/2} \frac{d\Gamma}{y_0 - y}. \quad (3.20)$$

The only unknown in this equation is the circulation, the integral is not very easy to handle, we will see how to compute it in next section.

3.2.3 The elliptic lift distribution (application type II)

Before starting, let's do a summery of what we have done. The line theory for a given wing is an integro-differential equation for $\Gamma(y_0)$, so the solution is $\Gamma(y_0)$. Then we can compute the local and total lift by:

$$L'(y_0) = \rho_\infty v_\infty \Gamma(y_0) \quad L = \int_{-b/2}^{b/2} L'(y) dy \quad (3.21)$$

and the local and total induced drag:

$$D'_i(y_0) = \Gamma(y_0) \epsilon(y_0) \quad D_i = \int_{-b/2}^{b/2} D'_i(y) dy \quad (3.22)$$

Now if we can assume a lift distribution on the wing, we can directly go throw the last equations. The elliptic circulation distribution is written:

$$\Gamma(y) = \Gamma_0 \sqrt{1 - \left(\frac{y}{b/2} \right)^2}. \quad (3.23)$$

where Γ_0 is the circulation in the plane of symmetry. Let's compute the velocity:

$$v(y_0) = \frac{1}{4\pi} \int_{-b/2}^{b/2} \frac{d\Gamma}{y_0 - y} = \frac{\Gamma_0}{2b} = cst \quad \Rightarrow \epsilon = \alpha_i = \frac{v(y_0)}{v_\infty} = \frac{\Gamma_0}{2bv_\infty} = cst. \quad (3.24)$$

where we used the transformation $y = b/2 \cos \theta$. We see that the induced angle of attack is constant along the span. We can compute $L'(y)$:

$$L'(y) = \rho v_\infty \sqrt{1 - \left(\frac{y}{b/2}\right)^2}. \quad (3.25)$$

On the other hand we can use (3.4) to express the lift as:

$$L'(y) = m(\alpha - \alpha_i - \alpha_0) \frac{1}{2} \rho_\infty v_\infty^2 c \quad (3.26)$$

Combining the equations we get:

$$(\alpha - \alpha_i - \alpha_0)c = \frac{2\Gamma_0}{v_\infty} \sqrt{1 - \left(\frac{y}{b/2}\right)^2}. \quad (3.27)$$

Note that if the left hand side is constant, the equation is satisfied for an **elliptic platform**. Since α_i is already constant, the whole term is constant only if the geometric angle of attack is constant and the profile does not change along the span. Since $C_{d_i} = C_L \alpha_i$, we can make the same analysis for the drag.

On the other hand, if the platform is non elliptic, since m varies little, the different angles must vary too. This is done by introducing a **twist** in the wing so that α varies. The lift coefficient is obtained by integration of the local lift:

$$\frac{1}{\frac{1}{2} \rho v_\infty^2 S} \int_{-b/2}^{b/2} L'(y) dy = \frac{\Gamma_0 \pi b}{2v_\infty S} = \frac{\Gamma_0 \pi}{2bv_\infty} AR. \quad (3.28)$$

Combination of this and what we found for α_i in this section we get:

$$\alpha_i = \frac{C_L}{\pi AR} \quad (3.29)$$

which is what we defined at the beginning of the chapter but for $e = 1$ (span efficiency factor). The induced drag is given by:

$$D'_i(y) = L'(y)\alpha_i \quad \Rightarrow C_{D_i} = C_L \alpha_i = \frac{C_L^2}{\pi AR}. \quad (3.30)$$

3.2.4 Wings with arbitrary distribution of the circulation

in this case we don't know a priori the lift distribution, we assume a serie:

$$\Gamma = \sum_{n=1}^N A_n \sin(n\theta). \quad (3.31)$$

Substitution of this in the Prandtl's fundamental equation gives:

$$\alpha(\theta_0) = \frac{1}{\pi v_\infty c(\theta_0)} \sum_n A_n \sin(n\theta_0) + \alpha_0(\theta_0) + \frac{1}{2\pi v_\infty b} \sum_n A_n n \int_\pi^0 \frac{\cos(n\theta)d\theta}{\cos\theta_0 - \cos\theta} \quad (3.32)$$

where we recognize the Glauert integral. We have here 1 equation for N unknowns A_1, \dots, A_N . We can find a solution by considering N equations for N points distributed along the span. Let's calculate the lift coefficient as for the previous section, by integrating:

$$C_L = \frac{1}{\frac{1}{2}v_\infty S} \int_{-b/2}^{b/2} \Gamma(y) dy = \frac{b}{u_\infty S} \sum_n \int_0^\pi A_n \sin(n\theta) \sin \theta d\theta = \frac{\pi b A_1}{2S v_\infty}. \quad (3.33)$$

For the induced drag we have:

$$C_{D_i} = \frac{1}{\frac{1}{2}v_\infty S} \int_{-b/2}^{b/2} \Gamma(y) \alpha_i dy. \quad (3.34)$$

Using (3.18), we can express $\alpha_i(\theta_0)$ as:

$$\alpha_i(\theta_0) = \frac{1}{2\pi v_\infty b} \int_\pi^0 \frac{\frac{d\Gamma}{d\theta}}{\cos \theta_0 - \cos \theta} d\theta = \frac{1}{2 \sin \theta_0 v_\infty b} \sum_n A_n n \sin(n\theta_0) \quad (3.35)$$

we can say that the induced drag is:

$$C_{D_i} = \frac{1}{2v_\infty^2 S} \int_0^\pi \sum_n \sum_k A_n A_k \sin(n\theta) \sin(k\theta) d\theta = \frac{\pi}{4v_\infty^2 S} \sum_n A_n^2 n \quad (3.36)$$

and using the lift coefficient:

$$C_{D_i} = \frac{C_L^2}{\pi AR} \left(1 + \sum_{n=2} \left(\frac{A_n}{A_1} \right)^2 \right) \Rightarrow e = \frac{1}{1 + \sum_{n=2} \left(\frac{A_n}{A_1} \right)^2} = \frac{1}{1 + \delta} \quad (3.37)$$

where δ is the **induced drag factor**, since it is always positive, $e < 1$.

Application 1: tapered wing

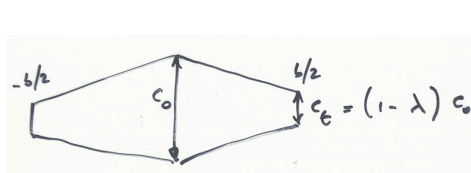


Figure 3.21

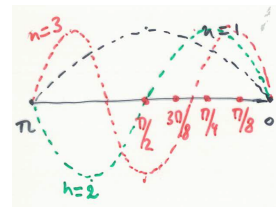


Figure 3.22

Same 2D profile along the span and no twist. Because of the symmetry, it is obvious that the pair n will have no contribution. Let's go until 7:

$$\Gamma = A_1 \sin \theta + A_3 \sin 3\theta + A_5 \sin 5\theta + A_7 \sin 7\theta. \quad (3.38)$$

To determine the coefficient we have to apply (3.32) to 4 points. Let's take half the span because of symmetry: $\theta = \pi/8, \pi/4, 3\pi/8, \pi/2$. Since the 2D profile is constant, α_0 is independent of θ , same for α since there are no twist.

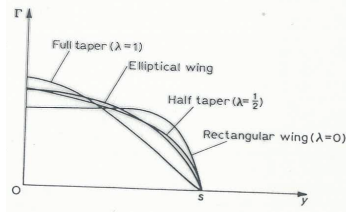


Figure 3.23

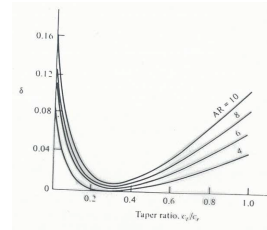


Figure 3.24

After some calculation one find a circulation distribution as in Figure 3.23, where λ is defined such that $c_t = (1 - \lambda)c_r$. $\lambda = 0$ corresponds to a rectangular wing and $\lambda = 1$ is the triangular one. Note that the figure also represents the lift. The lift coefficient no, because it becomes larger at the tips due to $c \searrow$. On Figure 3.24 is represented the induced drag coefficient δ . We see that it is always possible to find the taper ratio to have the minimum drag. Most of the planes use tapered wings since it is more simple to produce than elliptic wing.

Application 2: a wing with twist

We have to distinguish:

- **Geometrical twist:** the slope of the chord varies along the span, if α decreases from root to top, we speak about **geometrical washout**.
- **Aerodynamic twist:** in this case we play with the geometry of the 2D airfoil, the camber. If the camber decreases from root to tip, we speak about **aerodynamic washout**.

For the calculations, it is similar to the tapered wing but this time α and/or α_0 varies with the points. In general, one finds that the geometrical washout decreases δ and therefor the induced drag, except at very low lift coefficients (high velocity the drag is already not so important).

Numerical treatment

Instead of series, we can use the numerical treatment. We divide the wing in a number of stations spread along the span. For a given α , one assumes a value for Γ in each of the stations. This allows to calculate the induced angle of attack via:

$$\alpha_i(\theta_0) = \frac{1}{4\pi v_\infty} \int_{-b/2}^{b_2} \frac{d\Gamma}{y_0 - y} \quad (3.39)$$

where the integral is now computed numerically. Knowing this angle, we can use the 2D lift curve to find the local lift coefficient. On the other hand we have from Kutta-Joukowski:

$$c_l(\theta_0) = \frac{\Gamma(\theta_0)}{\frac{1}{2}v_\infty c(\theta_0)} \quad (3.40)$$

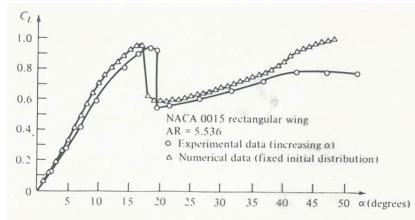


Figure 3.25
method can be used at stall, since we make use of the 2D curves. One has to be cautious since

where we know c_l , so we get a new $\Gamma(\theta_0)$ different from the postulated one. This leads to a new circulation:

$$\Gamma = \Gamma_{old} + \omega(\Gamma_{new} - \Gamma_{old}) \quad (3.41)$$

where ω is an underrelaxation factor to stabilize the method (≈ 0.05). The new Γ gives a new distribution of the induced angle and we repeat the method until the convergence. This

there is important 3D effects when separation.

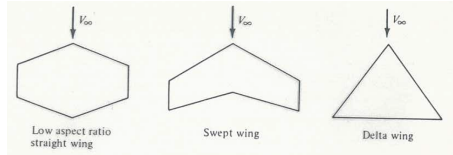


Figure 3.26

The lifting line theory gives good results for wings of more or less rectangular shape and average to high AR. For higher velocities however one frequently uses swept wings: the entire wing is placed at an angle with regard to the flow direction. Our theory is not as accurate as needed for the shapes shown on the figure. We have to use the **lifting surface theory**.

Chapter 4

Viscous and turbulent effects

4.1 Skin friction

We have already seen that the drag is caused by first the pressure distribution (form drag) and also by the viscous stresses (skin friction drag). At small α the skin friction represents 80-90% of the total drag and at stall conditions it is the form drag.

The form drag is also consequence of the viscous effects, the boundary layer due to viscous effect influences the pressure distribution. The viscous flow can be interpreted as the inviscid flow around an effective profile corrected with its boundary layer. In general this effective wing changes with α , has a smaller camber than the real wing so that the lift curve has a smaller slope than the inviscid with C_L smaller up to 10% for $Re = 10^6$. AC goes closer to the leading edge.

4.1.1 Laminar flow

Consider a flat plate at $\alpha = 0$ and incompressible flow, previous courses give a skin friction of:

$$C_f = \frac{1}{0.5\rho_\infty V_\infty^2 c} \int_0^c \tau_w dx = \frac{1.328}{\sqrt{Re_c}} \quad Re_c = \frac{V_\infty c}{\nu} \quad (4.1)$$

The boundary layer thickness δ is given by:

$$\delta(x) = \frac{5x}{\sqrt{Re_x}} \quad (4.2)$$

If the flow is compressible, the Mach number will play a role and the Prandtl number will appear as we have to take into account the energy equation for Navier-Stokes:

$$Pr = \frac{\mu C_p}{\kappa} \quad (4.3)$$

In incompressible flow the temperature of the flow remained more or less constant, this is not the case here, the boundary conditions on the plate (temperature) will influence the results. The skin friction and the boundary thickness become:

$$C_f = \frac{1.328}{\sqrt{Re_c}} F \left(M_\infty, Pr, \frac{T_w}{T_\infty} \right) \quad \delta = \frac{5x}{\sqrt{Re_x}} G \left(M_\infty, Pr, \frac{T_w}{T_\infty} \right) \quad (4.4)$$

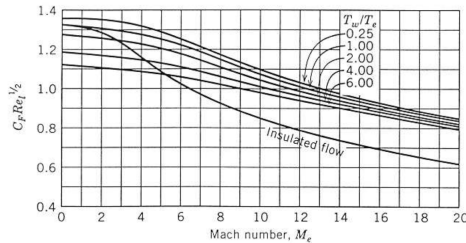


Figure 4.1

The functions F and G are found numerically. Here are plotted for several temperature and Mach numbers the skin friction over an adiabatic flat plate. One notice that the friction decreases with temperature of the wall and with Mach number.

Below is plotted the effect of the temperature on the velocity field and the temperature distribution in the boundary layer. One can see that the increase of T_w decreases $\frac{du}{dy}$ and so the friction $\tau_w = \mu(\frac{du}{dy})$. We also see that δ increases. On the right figure, we see that the δ increases with increasing Mach number for constant Re number. Increasing Re number decreases the friction.

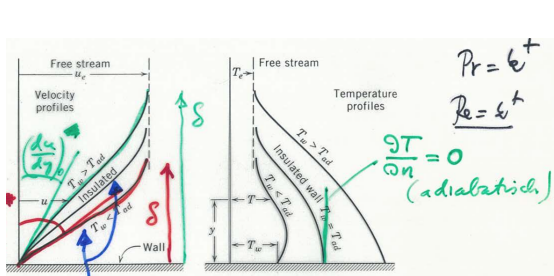


Figure 4.2

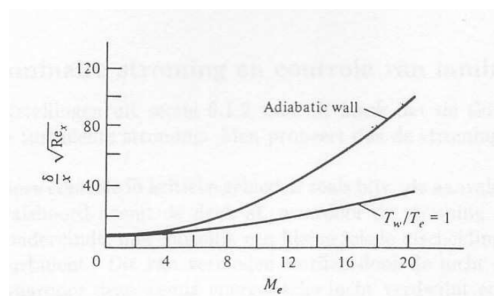
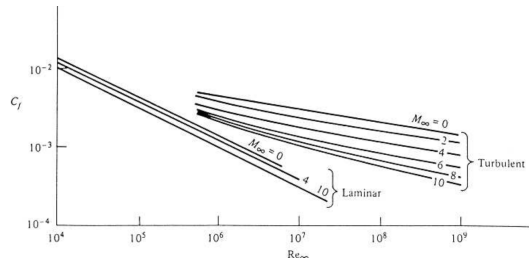


Figure 4.3

4.1.2 Turbulent flow



is higher than laminar).

Figure 4.4

The formula now are:

$$C_f = \frac{0.074}{Re_c^{1/5}} \quad \delta = \frac{0.37x}{Re_x^{1/5}} \quad (4.5)$$

and one can see on the plot that the turbulent flow has a larger friction for the same Re and C_f decreases with Mach number (the decrease

4.2 Methods to reduce the drag

4.2.1 Natural laminar flow and control of laminar flow

As the friction in laminar flow is lower than in turbulent, one tries to keep the flow like that as possible. We have to place an active control in critical areas like the leading edge. When the air accelerates, the pressure decreases and there is a positive pressure gradient pushing from backward and leading to small separation. When the flow reattaches, it becomes turbulent. This is avoided by sucking away the air in the boundary layer (slots or porous wing) as a result of what the low energy air disappears. For laminar flows, one tries to use **adapted wing profiles** and not active control. The wing profile has to be as smooth as possible and the lower pressure point as far downstream from the LE as possible. With this aim, the NACA 6 series has been developed.

For example the NACA 65-218 has a point of min pressure at 0.5 chord downstream of the LE, the design lift coefficient 0.2 and thickness of 18%.

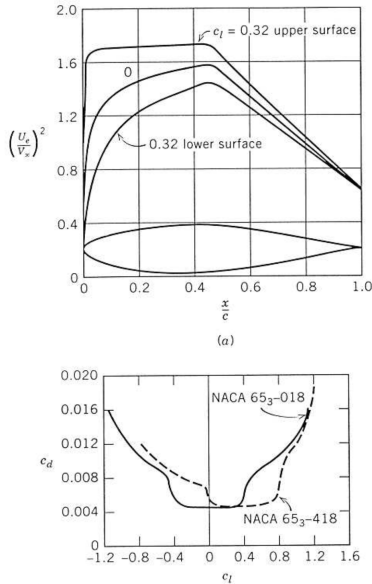


Figure 4.5

4.2.2 Reduction of the drag in turbulent flows

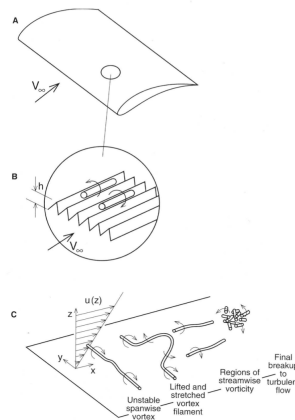


Figure 4.6

An advantage of turbulent flow is that it resists better to separation, so it is preferred in reverse gradient areas. To reduce the drag, we introduce **riblets** in the flow direction. This is illustrated on (c), the velocity distribution in the boundary layer induces spanwise vortices in the y direction, which is unstable. Because of its instability, it is deformed and lifted away from the wall. Because of this it breaks down and induces vortices in the flow direction which disintegrate and result in turbulent flow. Riblets have a stabilizing effect, they delay the transition to turbulent and make the flow in the viscous layer less chaotic when turbulent, so reducing drag.

The maximum drag reduction for profile 13R is 7-8% obtained for $s^+ \approx 15$ and 33 reduction of $\approx 2\%$.

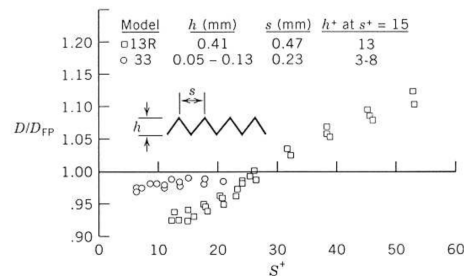


Figure 4.7

Chapter 5

The complete plane: additional components

5.1 High lift devices

The main objective of lift is to counterbalance the weight:

$$W = L = C_L \frac{1}{2} \rho_\infty V_\infty^2 S. \quad (5.1)$$

Suppose now that $V_\infty \ll$, there are 2 options to increase lift: increasing C_L or increasing S . The problem is that the 2 solutions increase the drag, the first need an increased camber, and for the second $D = C_D \frac{1}{2} \rho_\infty V_\infty^2 S$. The best solution is to increase C_L only for $V_\infty \ll$ and this can be done by changing the geometry or by controlling the boundary layer (attached flow).

5.1.1 Trailing edge flaps

Plain flap

The principle of flaps is to increase the camber. This is the most simple, the trailing edge shifts downward, increasing C_L . The characteristics are:

- Because of separation appearing earlier $\alpha_{stall} \searrow$, this is better for the view of the pilot.
- $C_L(\max)$ is up to 50% higher, reached for high deflection $\approx 80^\circ$.
- The drag increases much more than the lift $C_L/C_D \nearrow$, this is good for landing as it helps to decelerate.
- Center of pressure at the trailing edge $\rightarrow \Delta C_m < 0$ (nose down).

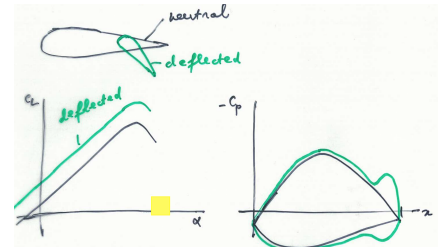


Figure 5.1

Split flap

- Separation appears later than the previous case, $\alpha_{stall} \searrow$ less.
- Larger wake because of the split \rightarrow more drag, not good for take off.
- $C_L(\max) \nearrow$ up to 60% and nose down less than previous case.



Figure 5.2

Slotted flap



In this case α_{stall} increases compared to plain because of the slot allowing the control of separation and the increase of C_D is smaller than the plain flap. $C_L(\max) \approx 65\%$.

Figure 5.3

Fowler flap

This is the most used type of flap, combination of the slotted flap and a backward motion:

- $C_L \nearrow$ further compared to slotted.
- $\alpha_{stall} \searrow$ compared to slotted because of $\frac{t}{c} \searrow$.
- $\Delta C_D \searrow$ because boundary layer control + $\frac{t}{c} \searrow$.
- $\Delta C_m \gg$ because flap going backward. In practice, the fowler flap contains many slots.



Figure 5.4

The figures below shows a good summary.

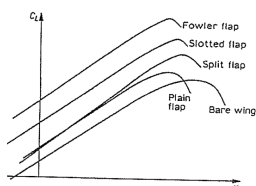


Figure 5.5

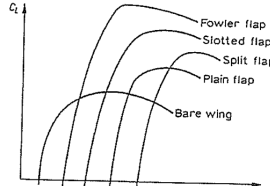


Figure 5.6

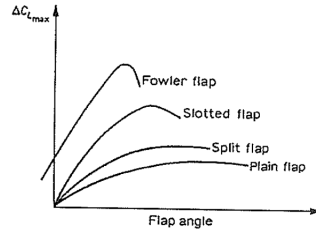


Figure 5.7

Remarks

- $\frac{dC_m}{dC_L} \approx cst$, this implies that k in $C_m = C_{m0} + kC_L$ does not change and that the **aerodynamic center** doesn't change.
- The flaps are placed near the fuselage, this decreases the efficiency, changes the lift distribution on the wing that have effect on D_i and the pressure center closer to the fuselage can have effects on the stability.
- Other types of flaps: Zap flap (split + fowler), C_L is higher than the split but the drag is higher than fowler.

5.1.2 Slat



Figure 5.8

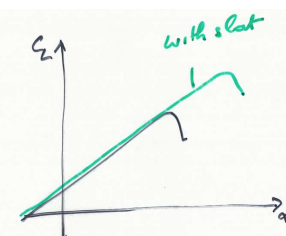


Figure 5.9

The slats are separated from the airfoil by a slot. This allows to energize the boundary layer by a flow through the slot. This has no effect for small $/alpha$, it allows to increase α_{stall} going from 15° to 25° , increasing $C_L(\max)$ up to 60%. The disadvantage is that for low speeds the

drag decreases (less detached boundary), this is bad for landing. And for higher speeds the flow disturbance increases the drag. **Controllable slats** are necessary.

The second disadvantage is that to have the lift increase effect we need to go to very high α , not good for the sight of the pilot.

5.1.3 Leading edge flap



Figure 5.10

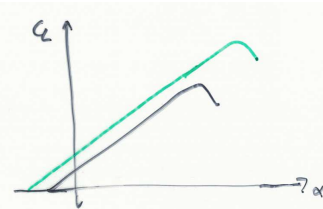


Figure 5.11

Deflection at high α can prevent LE separation, and this even more for high velocity wings with sharp LE. The lift coefficient increases because of increased camber, but the α_{stall} is less than the slat. Indeed all of these are used together nowadays.

5.2 Boundary layer control

Boundary layer blowing We saw previously that it was possible to energize the boundary layer by injecting high speed air through slots. This makes increase α_{stall} and the high velocity increases the circulation, thus $L \propto \alpha$.

Boundary layer suction This consists in sucking away the low velocity air by means of porous wings or suction holes.

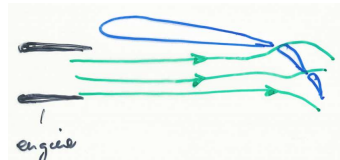


Figure 5.12

Remark For vertical or short take off and landing, the engine jet is used. The air coming from the engine is redirected to energize the boundary layer. VTOL: jet engine is deflected vertically for vertical take off, where the thrust must be equal to the weight, while it is about 30% for horizontal take off.

5.3 Tailplanes

Consider α small so that the lift is assumed perpendicular to the chord, applied on the AC and the weight is applied on the center of gravity. The moment in the center of gravity is:

$$C_m = C_{M_0} + C_L(h - h_0) \quad \Rightarrow \frac{dC_m}{dC_L} = h - h_0 > 0. \quad (5.2)$$

And since $dC_L/d\alpha = m$:

$$\frac{dC_m}{d\alpha} = m(h - h_0) > 0 \quad (5.3)$$

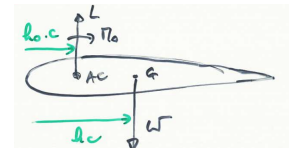


Figure 5.13

and the wing is **statically unstable** because the increase in α causes an increase in C_m and so even more nose up. We see that in fact the wing alone is stable only if the center of gravity is upstream of the aerodynamic center. **Tail** planes are used to increase stability, one has now:

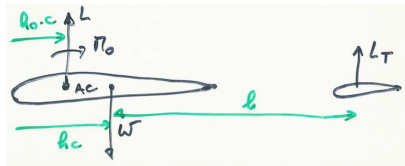


Figure 5.14

$$\frac{dC_m}{d\alpha} = m(h - h_0) - \frac{C_{L_T}}{da} \gamma \quad (5.4)$$

where $\gamma = \frac{lS_T}{cS}$ as $C_{L_T} = \frac{L_T}{0.5\rho_{\infty}V_{\infty}^2 S_T}$. One can reach stability for sufficiently high γ , by increasing l or S_T .

An alternative to tail planes are the **cannards** as illustrated here.

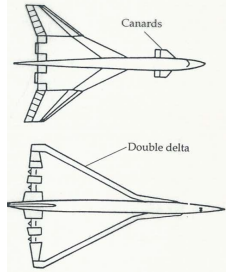


Figure 5.15

Chapter 6

2D wings in compressible flow

6.1 Subsonic flows

6.1.1 The Prandtl-Glauert relation

Remind that we have defined a potential function to describe incompressible flows, conservation of mass giving:

$$\vec{v} = \nabla\phi \quad \frac{\partial u}{\partial x} + \frac{\partial v}{\partial y} = 0 = \frac{\partial^2\phi}{\partial x^2} + \frac{\partial^2\phi}{\partial y^2}. \quad (6.1)$$

This can also be used to describe compressible flows, conservation of mass is then:

$$\rho(\phi_{xx} + \phi_{yy}) + \rho_x\phi_x + \rho_y\phi_y = 0 \quad (6.2)$$

where we introduced the shorthand notation $\frac{\partial a}{\partial x} = a_x$. We assume that the flow is isentropic, this is satisfied by inviscid flows (no shock wave):

$$\frac{\rho}{T^{\frac{1}{\gamma-1}}} = cst \quad \Rightarrow \frac{d\rho}{\rho} = \frac{1}{\gamma-1} \frac{dT}{T} \quad (6.3)$$

if the flow does not work (turbine), the temperature is constant and the equation becomes:

$$d\rho = -\frac{\rho}{2a^2}d(u^2 + v^2). \quad (6.4)$$

If we replace the velocities we get:

$$\rho_x = -\frac{\rho}{a^2}(\phi_x\phi_{xx} + \phi_y\phi_{xy}) \quad \rho_y = -\frac{\rho}{a^2}(\phi_x\phi_{xy} + \phi_y\phi_{yy}). \quad (6.5)$$

That we can substitute in (6.2):

$$\left(1 - \frac{1}{a^2}\phi_x^2\right)\phi_{xx} + \left(1 - \frac{1}{a^2}\phi_y^2\right)\phi_{yy} - \frac{2}{a^2}\phi_x\phi_y\phi_{xy} = 0. \quad (6.6)$$

We can now apply this to an airfoil, if the far field velocity profile is $u = V_\infty$, we can note the velocity field by means of perturbations: $u = V_\infty + \hat{u}$, $v = \hat{v}$. A perturbation potential function can be defined:

$$\phi = V_\infty x + \hat{\phi} \quad \text{with} \quad \hat{\phi}_x = \hat{u}, \quad \hat{\phi}_y = \hat{v}. \quad (6.7)$$

By substitution of this in (6.6):

$$\left[a^2 - (V_\infty + \hat{\phi}_x)^2 \right] \hat{\phi}_{xx} + \left[a^2 - \hat{\phi}_y^2 \right] \hat{\phi}_{yy} - 2(V_\infty + \hat{\phi}_x) \hat{\phi}_y \hat{\phi}_{xy} = 0. \quad (6.8)$$

Since the total temperature is constant:

$$\frac{a_\infty^2}{\gamma - 1} + \frac{V_\infty^2}{2} = \frac{a^2}{\gamma - 1} + \frac{(V_\infty + \hat{u})^2}{2} = \hat{v}^2 \quad (6.9)$$

If we make the assumption of small perturbation, the quadratic terms cancel and (6.8) and (6.9) become:

$$\begin{aligned} \frac{a_\infty^2}{a^2} &= 1 - (\gamma - 1) \frac{\hat{u}}{V_\infty} M_\infty^2 \\ \left[a^2 - V_\infty^2 + 2V_\infty \hat{u} \right] \hat{\phi}_{xx} + a^2 \hat{\phi}_{yy} - 2V_\infty \hat{v} \hat{\phi}_{xy} &= 0 \\ \Rightarrow \left[1 - M_\infty^2 - (\gamma + 1) M_\infty \frac{\hat{u}}{V_\infty} \right] \hat{\phi}_{xx} + \left[1 - (\gamma - 1) M_\infty^2 \frac{\hat{u}}{V_\infty} \right] \hat{\phi}_{yy} - 2M_\infty^2 \frac{\hat{v}}{V_\infty} \hat{\phi}_{xy} &= 0 \end{aligned} \quad (6.10)$$

where the last expression is obtained by dividing by a_∞^2 and replacing. By considering again the small perturbation ($V_\infty \ll$) equation we get the:

Transonic small perturbation potential equation

$$\left[(1 - M_\infty^2) - (\gamma + 1) M_\infty^2 \frac{\hat{\phi}_x}{V_\infty} \right] \hat{\phi}_{xx} + \hat{\phi}_{yy} = 0. \quad (6.11)$$

We can see that the \hat{u} appears in $\hat{\phi}_{xx}$ term, this is no longer negligible for **sonic** velocities. For sub- and super-sonic flows however the equation simplifies in:

$$(1 - M_\infty^2) \hat{\phi}_{xx} + \hat{\phi}_{yy} = 0. \quad (6.12)$$

Note that we retrieve our incompressible equation for $M_\infty \rightarrow 0$. Be aware that this last relation is only valid for small perturbations (small bodies in practice) and sub- or super-sonic flows ($M_\infty > 1.2$, $M_\infty < 0.8$).

Let's now operate a change of coordinate $(x, y) \rightarrow (\xi, \eta)$, recalling $1 - M_\infty^2 \equiv \beta^2$:

$$\xi = x \quad \eta = \beta y \quad \bar{\phi}(\xi, \eta) = m \cdot \hat{\phi}(x, y) \quad (6.13)$$

where m is a constant. Let's find the expression of $\bar{\phi}(\xi, \eta)$. The chain rule gives:

$$\begin{aligned} \hat{\phi}_x &= \hat{\phi}_\xi = \frac{1}{m} \bar{\phi}_\xi & \hat{\phi}_y &= \frac{\beta}{m} \bar{\phi}_\eta & \hat{\phi}_{xx} &= \frac{1}{m} \bar{\phi}_{\xi\xi} & \hat{\phi}_{yy} &= \frac{\beta^2}{m} \bar{\phi}_{\eta\eta} \\ \Rightarrow \bar{\phi}_{xx} + \bar{\phi}_{yy} &= 0 \end{aligned} \quad (6.14)$$

We can see that the compressible flow in (x, y) is reduced to an incompressible flow in the (ξ, η) plane. Pay attention that $\bar{\phi}$ describes the perturbation velocities \bar{u}, \bar{v} in the (ξ, η) plane.

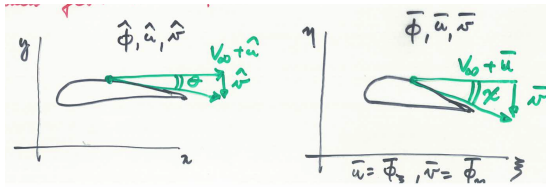


Figure 6.1

We can now focus on the shape of the profile in the new axis. Let's analyze the tangent to the profile by defining the angle θ for the profile in (x,y) . Under the assumption of small perturbation (thin airfoil), we can see that:

$$\tan \theta \approx \theta = \frac{\hat{v}}{V_\infty + \hat{u}} \approx \frac{\hat{v}}{V_\infty} = \frac{1}{V_\infty} \hat{\phi}_y \quad \Rightarrow \chi \approx \frac{1}{V_\infty} \bar{\phi}_\eta \quad (6.15)$$

where the analogy for the new plane is done. Using (6.14), we get:

$$\theta = \frac{\beta}{m} \chi. \quad (6.16)$$

Let's investigate two cases:

- If we choose $m = \beta$, $\theta = \chi$, the two profiles are identical. We have for the velocity:

$$\hat{u} = \hat{\phi}_x = \frac{\bar{\phi}_\xi}{\beta} = \frac{\bar{u}}{\beta} \quad (6.17)$$

and since the pressure coefficient is given by $C_p = -\frac{2\hat{u}}{V_\infty}$:

Prandtl-Glauert rule

$$C_p = \frac{C_{p,inc}}{\beta} = \frac{C_{p,inc}}{\sqrt{1 - M_\infty^2}}. \quad (6.18)$$

This equation allows us to compute the pressure distribution in compressible flow, beginning from the incompressible one.

Since the lift and moment coefficient are given by the integration of the pressure coefficient along the wing, we have the same result for them (so also the slope of lift curve m). Here is plotted the experimental data and the approximated m by means of the above relation for $\alpha = 0$ and for different airfoil thickness τ . We can see that for the thinner wings, we have a good agreement, until we reach the **critical Mach number** (Mach number at infinity for which Mach number 1 is reached on the profile). This value exceeded, we have shock waves (formula valid only for Mach until 0.8). For thicker wings, we see that the slope m is always underestimated. The critical Mach number is here much lower.

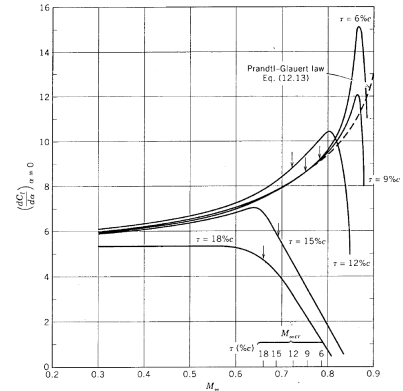


Figure 6.2

- If we choose $m = 1$, $\hat{u} = \bar{u}$ so that $C_p = C_{p,inc}$. We see that the pressure coefficient is now the same but the profiles are different following we are in the compressible or incompressible case $\theta = \beta\chi$.



The angle relation must be true along the entire profile, particularly at the maximum thickness:

$$\tau = \beta\tau_{inc}. \quad (6.19)$$

Figure 6.3

Remark 1 If we take into account the aspect ratio, we can rewrite the slope m as:

$$m = \frac{m_{inc}}{\beta} \frac{2\pi}{\beta \left(1 + \frac{2}{eAR}\right)} \quad (6.20)$$

where we used the theoretical 2D slope 2π . Another possibility is to write the lift as:

$$c_l = \frac{2\pi}{\beta} (\alpha - \alpha_{L_0} - \alpha_i) = \frac{2\pi}{\beta + \frac{2}{eAR}} (\alpha - \alpha_{L_0}) \quad (6.21)$$

We can last note the existence of the DATCOM formula that accounts for the effect of the aspect ratio, sweep angle Λ , Mach number and has also a correction factor for viscous effects $\kappa \approx 0.97$:

$$m = \frac{2\pi AR}{2 + \sqrt{\frac{AR^2 + beta^2}{\kappa^2} \left(1 + \frac{\tan^2 \Lambda}{\beta^2}\right) + 4}}. \quad (6.22)$$

Remark 2 We can also rearrange the expression of C_p with the approximation of small angles, we had:

$$C_p = \frac{p - p_\infty}{\frac{1}{2} \rho_\infty V_\infty^2} = \frac{\gamma 2 p_\infty}{\gamma \rho_\infty V_\infty^2} \left(\frac{p}{p_\infty} - 1\right) = \frac{2}{\gamma M_\infty^2} \left(\frac{p}{p_\infty} - 1\right) \quad \gamma \frac{p_\infty}{\rho_\infty} = \gamma r T = a^2 \quad (6.23)$$

The isentropic flow and the constant T_c give:

$$\begin{aligned} \frac{p}{p_\infty} &= \left(\frac{T}{T_\infty}\right)^{\frac{\gamma}{\gamma-1}} = \left(\frac{T_t - \frac{1}{2c_p} [(V_\infty + \hat{u})^2 + \hat{v}^2]}{T_\infty}\right)^{\frac{\gamma}{\gamma-1}} \quad T_t = T_\infty + \frac{V_\infty^2}{2c_p} \\ \Rightarrow \frac{p}{p_\infty} &= \left[1 - \frac{\gamma-1}{2} M_\infty^2 \left(\frac{2\hat{u}}{V_\infty} + \frac{\hat{u}^2 + \hat{v}^2}{V_\infty^2}\right)\right]^{\frac{\gamma}{\gamma-1}} = 1 - \frac{\gamma}{2} M_\infty^2 \left(\frac{2\hat{u}}{V_\infty} + \frac{\hat{u}^2 + \hat{v}^2}{V_\infty^2}\right) + \dots \end{aligned} \quad (6.24)$$

where the last expression comes from the fact that the second term is small so that we have the Taylor development of $1 + \epsilon$ (first order limited). We can neglect the second term in bracket since we have small perturbation square, and we get by (6.23):

$$\frac{p}{p_\infty} = -\frac{2\hat{u}}{V_\infty} \quad (6.25)$$

6.1.2 Improved corrections for compressibility

With the increasing cruise speed of WW2, we have 2 more precise relations:

Karman-Tsien relation

$$C_p = \frac{C_{p,inc}}{\sqrt{1 - M_\infty^2} + \frac{M_\infty^2}{1 + \sqrt{1 - M_\infty^2}} \frac{C_{p,inc}}{2}} \quad (6.26)$$

or the more recent:

Laitone relation

$$C_p = \frac{C_{p,inc}}{\sqrt{1 - M_\infty^2} + \frac{M_\infty^2 (1 + \frac{\gamma-1}{2} M_\infty^2) C_{p,inc}}{2\sqrt{1 - M_\infty^2}}} \quad (6.27)$$

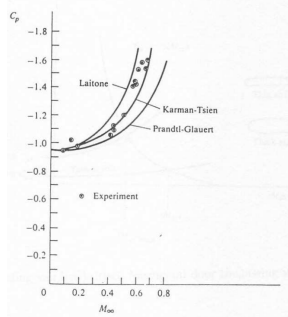


Figure 6.4

We can see experimental results here, using these coefficient we match better the lower values.

6.1.3 The critical Mach number

By definition, it is the M_∞ when $M = 1$ somewhere on the airfoil. Consider a point A, the drag is given by:

$$C_{p,A} = \frac{2}{\gamma M_\infty^2} \left(\frac{p_A}{p_\infty} - 1 \right) \quad (6.28)$$

If we combine the fact that the flow is isentropic:

$$\frac{p_A}{p_\infty} = \left(\frac{T_A}{T_\infty} \right)^{\frac{\gamma}{\gamma-1}} = \left(\frac{1 + \frac{\gamma-1}{2} M_\infty^2}{1 + \frac{\gamma-1}{2} M_A^2} \right)^{\frac{\gamma}{\gamma-1}} \Rightarrow C_{p,A} = \frac{2}{\gamma M_\infty^2} \left[\left(\frac{1 + \frac{\gamma-1}{2} M_\infty^2}{1 + \frac{\gamma-1}{2} M_A^2} \right)^{\frac{\gamma}{\gamma-1}} - 1 \right] \quad (6.29)$$

If now we consider $M_\infty = M_{kr} \rightarrow M_A = 1$, so that the equation becomes:

$$C_{p,A} = \frac{2}{\gamma M_\infty^2} \left[\left(\frac{1 + \frac{\gamma-1}{2} M_\infty^2}{1 + \frac{\gamma-1}{2} M_A^2} \right)^{\frac{\gamma}{\gamma-1}} - 1 \right] \quad C_{p,A} = \frac{C_{p,A,inc}}{\sqrt{1 - M_{kr}^2}}, \quad (6.30)$$

where the second equation is the Prandtl-Glauert relation. We can plot the two equations on a graph. The intersection of the two graphs gives the critical Mach number. We can see that the minimum lift coefficient at low velocities is more negative than the thin case, characterized by a smaller M_{kr} . The perturbation of the flow is higher. Flying at high subsonic velocities is important \rightarrow thin airfoil. When the angle of attack increases, the lift increases but the higher velocity on the suction part makes the M_{kr} much lower. We want so the wing to be as thin as possible but we are limited by the structural strength and the fuel storage.

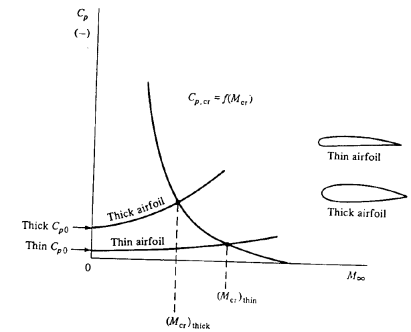


Figure 6.5

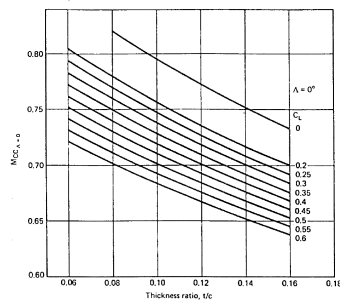


Figure 6.6

We avoid also large bending of the leading edge to avoid large accelerations. One solution to increase M_{kr} is to place the maximum camber downstream, about 50% of the chord because the velocities on the suction side will be lower. Placing it too downstream will create a too high opposite gradient and cause separation.

Symmetrical wings have a larger M_{kr} , however be careful with combination of sharp LE because of LE separation. In practice we have a quasi-symmetrical profile with camber near LE. **Swept** wings also increase the M_{kr} .

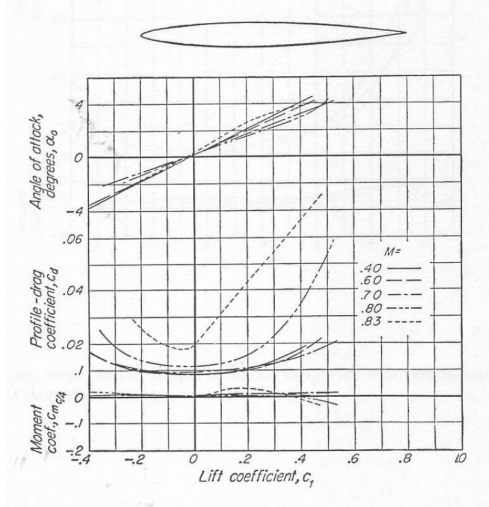


Figure 6.7

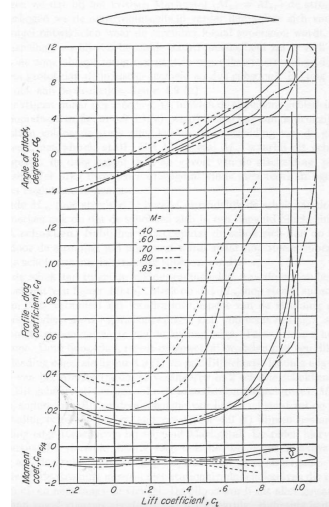


Figure 6.8

We can observe here above, the plot of α , C_L and C_D for a symmetrical and a non-symmetrical airfoil. We can observe on Figure 6.7 that the slope of the lift curve goes up to $M = 0.83$ (Prandtl-Glauert). Once above M_{kr} it starts to decrease and the drag suddenly increases.

On Figure 6.8 we can see similar effects at the difference that around M_{kr} we have a positive increase of the zero lift angle, having a negative effect on longitudinal stability. Note that the decrease of the lift curve starts earlier, M_{kr} is smaller.

6.2 Transonic flows

6.2.1 Drag divergence Mach number

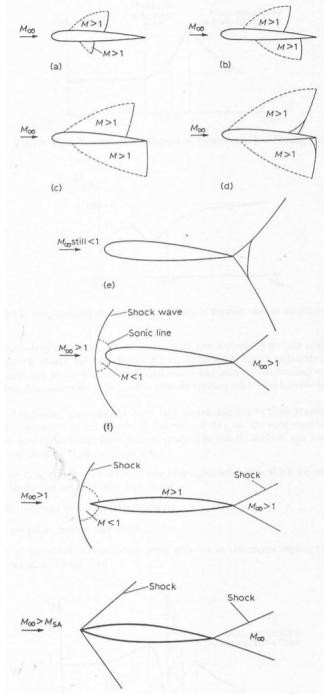


Figure 6.9

At the critical Mach number $M_\infty = M_{cr}$, the flow reaches $M = 1$ somewhere on the wing. If the velocity at ∞ is increased, M_∞ also (still <0), a small area where the flow becomes **supersonic** will develop on the **suction side**. For increasing M_∞ this area will grow and at a certain M_∞ a **shock wave** will develop, as a result of which the flow will become **subsonic** again (the supersonic area abruptly terminated). Such area also develops on the **pressure side** at high M_∞ (Figure 6.9 (a)).

If M_∞ increases further, the supersonic regions further extends and the shock waves move downstream, the one on the pressure side more rapidly (Figure 6.9 (b) (c)). As soon as the shock waves are strong enough, they can cause separation of the boundary layer, this separation is the **shock stall** and the M_∞ where this happens is called the **drag divergence Mach number**. Indeed, the drag suddenly increases as a result of the separation, this called **transonic drag rise**, shown on Figure 6.10.

For further increase of $M_\infty < 1$, the shock wave on the pressure side eventually reaches the trailing edge (Figure 6.9 (d)). In a certain Mach number range, the shock wave manifests the so-called

λ shocks. Near the profile the shock has two legs, a first oblique one through which the flow is slowed down but remains supersonic, and a second normal one through which the flow becomes subsonic.

Eventually the shock wave on the suction side can also reach the trailing edge and give birth to the **bifurcated trailing edge shock pattern** (Figure 6.9 (e)).

For further increase of M_∞ there is no change, till M_∞ exceeds 1. In this case, a so-called **detached bow shock** develops upstream of the leading edge. There is a small subsonic region between this shock and the leading edge. This manifests both for thick, bounded leading edge and thin one (Figure 6.9 (f) (g)). In the second case, the bow shock changes into 2 oblique shocks at the leading edge for increasing M_∞ (Figure 6.9 (h)). This happens at the **shock attachment Mach number, M_{SA}** . For further M_∞ , the flow becomes fully supersonic and the drag decreases. In the case of rounded leading edge, the bow shock continues to exist and comes closer to the leading edge.

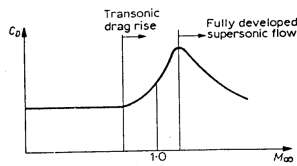


Figure 6.10

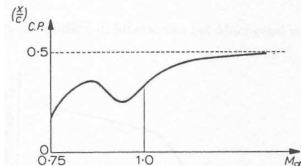


Figure 6.11

Under transonic conditions the flow is non-stationary, the shock waves moves up and down on the wing. The pilot senses this as **buffeting** (response of the structure to aerodynamic excitation) and vibrations. This can make the plane uncontrollable or cause serious damages. The cause of the excitation is the fluctuating pressure in non-stationary conditions. Normally one flies under the buffeting margin but one can exceed it in case of sudden maneuvers for fighters for example.

The center of pressure is also moving with M_∞ (Figure 6.11). First, it goes backward as the shock wave going backward on the suction side makes the underpressure greater. Then, it goes forward because the shock wave on the pressure side is moving faster. The latter reaches the trailing edge while the shock wave on the suction side still moves backward, making the center of pressure again move backward, tending to the 50% chord. This makes the control of the plane more difficult.

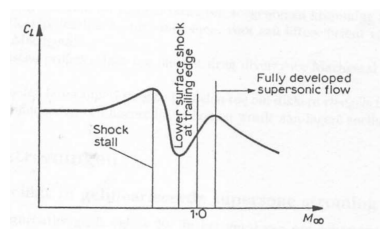


Figure 6.12

It is this buffeting effect that imposes an upper limit to the velocity of subsonic planes. With the increase of the drag due to separation when shock waves (shock-stall) is associated a decrease of the lift. We can see that the lift temporary increases after the lower shock reaches the trailing edge. This is explained by the smaller separation when in this location. The drag divergence Mach number is 5-10% larger than M_{cr} .

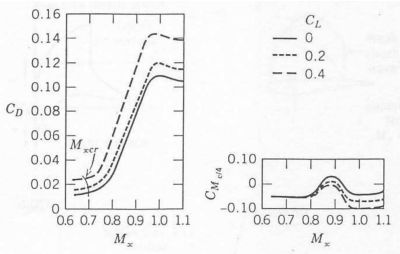


Figure 6.13

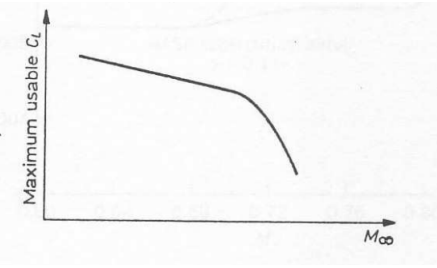


Figure 6.14

On Figure 6.13 we can see the influence of increasing lift (increasing α). We can notice that with increasing lift, the drag increases for all Mach numbers, the moment increases in the transonic region and M_{cr} decreases. On Figure 6.14, we notice that the lift coefficient strongly decreases in the transonic region due to buffering effects.

6.2.2 Supercritical wings

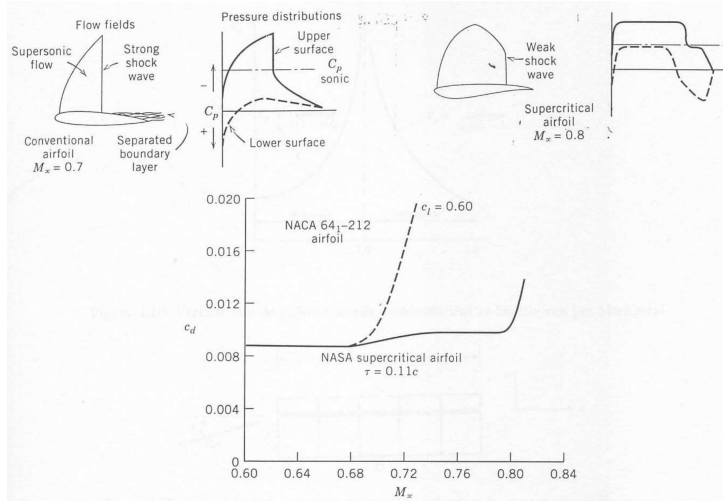


Figure 6.15

closer to the trailing edge.

For subsonic wings, it is thus desired to have the largest drag divergence Mach number possible. This can be achieved by using high critical Mach number wings, or increase the difference $M_{div} - M_{cr}$. The second solution led to the supercritical wings. These have a rather flat suction side to limit the acceleration of the flow, keeping the supersonic speeds lower than other profiles and limit the strength of the shock that creates less drag. The comparison between the two type of wings is done on Figure 6.15. We can see that the M_{cr} is higher and the weaker shock wave

The new shape of the suction side has a negative effect on the lift, this is compensated by an increased curvature on the pressure side near the trailing edge. On the figure we can see that the use of critical wings increases the drag divergence Mach number, that can go up to 0.99. These allows the use of thicker wings, allowing more fuel storage at lower speeds.

6.3 Supersonic flows

6.3.1 The drag coefficient in a linearized supersonic flow

The potential equation we used in the framework of potential equation can be rewritten in the case of supersonic flow as:

$$(1 - M_\infty^2) \hat{\phi}_{xx} + \hat{\phi}_{yy} = 0 \quad \Rightarrow \lambda^2 \hat{\phi}_{xx} - \hat{\phi}_{yy} = 0. \quad (6.31)$$

The linearized potential equation corresponds to the wave equation with $\lambda^2 = M_\infty^2 - 1 > 0$. We can show that the solution of this equation is

$$\hat{\phi}(x, y) = f(x - \lambda y) = \hat{\phi}_1(x - \lambda y) + \hat{\phi}_2(x + \lambda y). \quad (6.32)$$

Let's define 2 families of characteristic curves:

$$\begin{cases} C^+ : x - \lambda y = cst & \Rightarrow y = \frac{1}{\lambda}x + cst = \frac{1}{\sqrt{M_\infty^2 - 1}}c + cst \\ C^- : x + \lambda y = cst & \Rightarrow y = -\frac{1}{\lambda}x + cst = -\frac{1}{\sqrt{M_\infty^2 - 1}}c + cst \end{cases} \quad (6.33)$$

In this way, $\hat{\phi}_1$ and $\hat{\phi}_2$ are respectively constant on C^+ and C^- .

The slope is denoted μ_∞^\pm for C^\pm such that:

$$\tan \mu_\infty^\pm = \pm \frac{1}{\sqrt{M_\infty^2 - 1}} \quad \sin \mu_\infty^\pm = \pm \frac{1}{M_\infty}. \quad (6.34)$$

To find the general solution in P, let's first consider the initial data given on the y-axis:

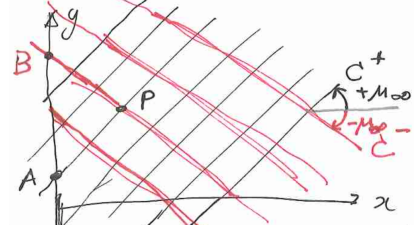


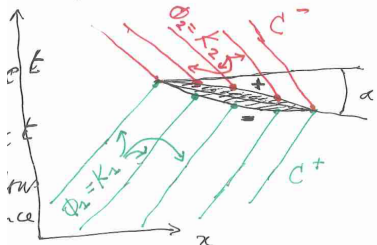
Figure 6.11
6.35

Now let's construct C^+ and C^- through P:

$$C^+ : x - \lambda y = x_A - \lambda y_A \quad C^- : x - \lambda y = x_B + \lambda y_B. \quad (6.36)$$

Finally, the solution in P is so given by:

$$\hat{\phi}(x_p, y_p) = \hat{\phi}(x_A - \lambda y_A) + \hat{\phi}_2(x_B + \lambda y_B) = F(x_A - \lambda y_A) + G(x_B + \lambda y_B) \quad (6.37)$$



Now let's define the initial conditions at $x = 0$ for small α for a thin profile:

$$F(y) = K_1 = cst \quad G(y) = K_2 = cst \quad \Rightarrow \hat{\phi} = cst \quad (6.38)$$

since the incoming flow is uniform. On the pressure side, we have $\hat{\phi}_1(x - \lambda y) = K_1$ which gives in the solution:

Figure 6.17

$$\hat{\phi}(q) = K_1 + \hat{\phi}_2(q) \quad \rightarrow \hat{\phi}_x = \frac{d\hat{\phi}_2}{dq} = \hat{u}^- \quad \hat{\phi}_y = \frac{d\hat{\phi}_2}{dq} \lambda = \hat{v}^- \quad \Rightarrow \hat{v}_{wall} = \lambda \hat{u}_{wall} \quad (6.39)$$

If we express the tangent as $\tan \theta_w \approx \theta_w = \frac{\hat{v}_w^-}{\hat{u}^- + V_\infty} \approx \frac{\hat{v}_w^-}{V_\infty}$, We can get by replacing the last results in the previous pressure coefficient equation for small perturbations:

Law of Ackeret

$$C_p^- = -\frac{2\hat{u}_w^-}{V_\infty} = -\frac{2\theta_w^-}{\sqrt{M_\infty^2 - 1}}. \quad (6.40)$$

The same reasoning can be done for the suction side where we'll get:

$$\hat{\phi}_x = \frac{d\hat{\phi}_1}{dq} = \hat{u}_w^+ \quad \hat{\phi}_x = \frac{d\hat{\phi}_1}{dq}(-\lambda) = \hat{v}_w^+ = -\lambda \hat{u}_w^+ \quad \Rightarrow C_p^+ = \frac{2\theta_w^+}{\sqrt{M_\infty^2 - 1}}. \quad (6.41)$$

Application to a flat plate

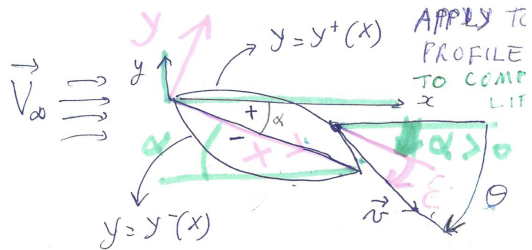


Figure 6.18

Consider the thin profile define by functions $y^+(x)$ and $y^-(x)$ with angles defines as:

$$\begin{aligned} \epsilon &= \frac{dy}{dx} < 0 & \theta &= \frac{\hat{v}}{\hat{u} + V_\infty} < 0 \\ \Rightarrow \theta &= \epsilon - \alpha = \frac{dy}{dx} - \alpha \end{aligned} \quad (6.42)$$

as $\alpha > 0$. We can then apply the last formula:

$$C_p^+ = \frac{2\theta_w^+}{\sqrt{M_\infty^2 - 1}} = \frac{2\left(\frac{dy^+}{dx} - \alpha\right)}{\sqrt{M_\infty^2 - 1}} \quad C_p^- = -\frac{2\theta_w^-}{\sqrt{M_\infty^2 - 1}} = \frac{2\left(\alpha - \frac{dy^-}{dx}\right)}{\sqrt{M_\infty^2 - 1}}. \quad (6.43)$$

We are now interested in computing the normal and tangential force applied on the wing, for a counter-clock contour:

$$C_N = \int_0^1 C_p^- \frac{dx}{c} + \int_1^0 C_p^+ \frac{dx}{c} = \frac{4\alpha}{\sqrt{M_\infty^2 - 1}} \quad (6.44)$$

where we replace the C_p 's by their definition and we neglect $\frac{dy}{dx}$ terms. For the drag we have the same procedure but by neglecting this time α :

$$\begin{aligned} C_\Gamma &= -\int_0^1 C_p^- \frac{dy}{c} - \int_1^0 C_p^+ \frac{dy}{c} = \frac{2}{\sqrt{M_\infty^2 - 1}} \left[\int_0^1 \left(\frac{dy^-}{dx} \right)^2 \frac{dx}{c} + \int_0^1 \left(\frac{dy^+}{dx} \right)^2 \frac{dx}{c} \right] \\ \Rightarrow C_\Gamma &= \frac{2}{\sqrt{M_\infty^2 - 1}} [I^- + I^+] \end{aligned} \quad (6.45)$$

To compute the lift and drag coefficient we only have to make the projections, and in case of flat plate $\frac{dy}{dx} = 0 = I^\pm$:

$$\begin{aligned} C_l &= -C_\Gamma \sin \alpha + C_N \cos \alpha \approx -\alpha C_\Gamma + C_N & C_d &= C_\Gamma + \alpha C_N \\ \Rightarrow C_l &= \frac{4\alpha}{\sqrt{M_\infty^2 - 1}} & C_d &= \frac{4\alpha}{\sqrt{M_\infty^2 - 1}}. \end{aligned} \quad (6.46)$$

Remind that the drag is the **wave drag**.

Application to a double wedge

If we apply the Ackeret law to this profile we have:

$$\begin{aligned} C_{p1} &= \frac{2(\delta - \alpha)}{\sqrt{M_\infty^2 - 1}} & C_{p2} &= \frac{2(\delta + \alpha)}{\sqrt{M_\infty^2 - 1}} \\ C_{p3} &= \frac{-2(\delta + \alpha)}{\sqrt{M_\infty^2 - 1}} & C_{p4} &= \frac{-2(\delta - \alpha)}{\sqrt{M_\infty^2 - 1}} \end{aligned} \quad (6.47)$$

We can compute the lift and drag coefficients by integrating over the surface:

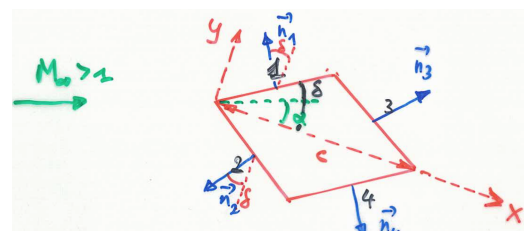


Figure 6.19

$$\vec{F} = - \oint p d\vec{S} = - \oint (p - p_\infty) d\vec{S} = - \frac{1}{2} \rho_\infty V_\infty^2 \oint C_p d\vec{S}$$

$$\Rightarrow \vec{F}_1 = - \frac{1}{2} \rho_\infty V_\infty^2 C_{p1} \frac{c}{2} \vec{n}_1$$
(6.48)

If we make the force non dimensional:

$$\vec{C}_1 = \frac{\vec{F}_1}{\frac{1}{2} \rho_\infty V_\infty^2 c} = - \frac{C_{p1}}{2} \vec{n}_1 \quad \Rightarrow \vec{C}_i = - \frac{C_{pi}}{2} \vec{n}_i$$
(6.49)

If we look to the normal and tangent forces we find:

$$C_y = \vec{C}_i \cdot \vec{i}_y = \left(-\frac{C_{p1}}{2} + \frac{C_{p2}}{2} - \frac{C_{p3}}{2} + \frac{C_{p4}}{2} \right) \cos \delta = \frac{4\alpha}{\sqrt{M_\infty^2 - 1}} \cos \delta \approx \frac{4\alpha}{\sqrt{M_\infty^2 - 1}}$$

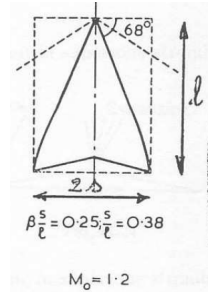
$$C_x = \vec{C}_i \cdot \vec{i}_x = \left(\frac{C_{p1}}{2} + \frac{C_{p2}}{2} - \frac{C_{p3}}{2} - \frac{C_{p4}}{2} \right) \sin \delta = \frac{4\delta}{\sqrt{M_\infty^2 - 1}} \sin \delta \approx \frac{4\delta^2}{\sqrt{M_\infty^2 - 1}}$$
(6.50)

Then we make the same projection as previously:

$$c_l \approx C_y - \alpha C_x = \frac{4\alpha}{\sqrt{M_\infty^2 - 1}} - \frac{4\delta^2 \alpha}{\sqrt{M_\infty^2 - 1}} \approx \frac{4\alpha}{\sqrt{M_\infty^2 - 1}}$$
(6.51)

We find thus the same lift coefficient as the flat plate. Let's see the drag:

$$c_d = C_x + \alpha C_y = \frac{4\alpha}{\sqrt{M_\infty^2 - 1}} + \frac{4\delta}{\sqrt{M_\infty^2 - 1}},$$
(6.52)



where the first term is **incidence wave drag** (result of lift), the same as the flat plate and the second term the **thickness wave drag** (result of volume) corresponding to the drag of the wedge at 0 degrees and angle of attack. The following empirical formula can be used for both drag on wing and on **complete plane**:

$$C_{Dw} = k_0 \frac{128}{\pi} \frac{V^2}{Sl^4} + k_1 \frac{1}{2\pi} \frac{S}{l^2} \lambda^2 C_L^2$$
(6.53)

where k_0 and k_1 are constant of order 1 depending on the geometry and l the average length as represented on the figure.

6.3.2 Supersonic wings

The flow properties are different from the subsonic case, as they are mainly given by shocks and expansions. Straight lines and sharp corners are as good as curved surfaces. Thus a flat plate is already the optimum theoretically, but there are structural constraints and fuel storage problems.

Camber is thus not appropriate for the supersonic case, as the zero lift angle of attack is positive (lift negative when $\alpha = 0$). The camber reduces the lift in all incidences when supersonic. Consequently, we mainly use **symmetrical wings**.

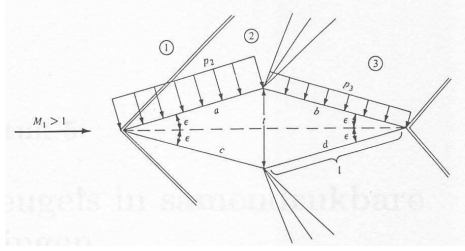


Figure 6.21

shocks and their expansion is called **wave drag**. When $\alpha \neq 0^\circ$ a lift arises, is comparable to the flat plate one but the drag is larger.

Another useful profile is the **biconvex profile**. Here both sides are circle arcs of same radius. The Prandtl-Meyer expansion of the double wedge is replaced by a range of **Mach waves** (expansion waves, ch8). The leading edge shock is bent, we have more drag than the double wedge for the same t/c ratio and approximately the same lift. The leading edge angle is larger, the Mach number must be higher before the shock to be attached to the LE.

This profile offers structural advantages and more fuel storage. In conclusion, in supersonic flight, we'd better have sharp leading edge to limit the shock drag, but this is not good for subsonic flight, take-off and landing as the stalling speed will be too low and the lift too.

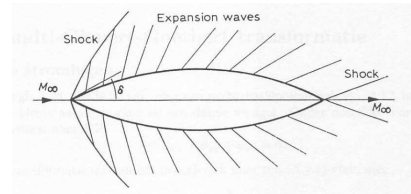


Figure 6.22

Chapter 7

3D wings in compressible flows

7.1 The Prandtl-Glauert-Goethert transformation

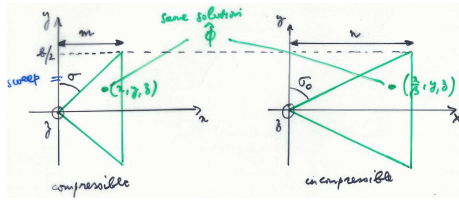
7.1.1 Subsonic flows

The previous potential equation can be extended into 3D into the same conditions like:

$$\beta^2 \hat{\phi}_{xx} + \hat{\phi}_{yy} + \hat{\phi}_{zz} = 0. \quad (7.1)$$

Then we apply the transformation of (x, y, z) to (X, y, z) with $X = \frac{x}{\beta}$ so that the previous equation becomes:

$$\hat{\phi}_{XX} + \hat{\phi}_{yy} + \hat{\phi}_{zz} = 0. \quad (7.2)$$



The flow in (x, y, z) is compressible with $M < 1$, when in (X, y, z) it is incompressible. The solution or ϕ in similar points (points x, y, z and $x/\beta, y, z$) is the same. This kind of transformation is represented on the figure. We remark that the leading edges sweep and the aspect ratios are related as:

Figure 7.1

$$\frac{\tan \sigma_0}{\sigma} = \frac{n}{m} = \frac{1}{\beta} \quad \frac{AR_0}{AR} = \frac{b_0^S}{b^2 S} = \frac{c}{c_0} = \beta. \quad (7.3)$$

The slope of the wing in the z -direction is the same in the two axis:

$$\tan \theta \approx \theta = \frac{\hat{w}}{\hat{u} + V_\infty} \approx \frac{\hat{w}}{V_\infty}. \quad (7.4)$$

The pressure coefficient for small perturbations is known:

$$C_p = -\frac{2\hat{\phi}_x}{V_\infty} = -\frac{1}{\beta} \frac{2\hat{\phi}_X}{V_\infty} = \frac{C_{p0}}{\beta}. \quad (7.5)$$

We obtain the same equation as in 2D, whereas now the profiles are not identical! For the lift on a section ($y = \text{cst}$), we can compute the integral:

$$L' = \frac{1}{2} \rho_\infty V_\infty^2 \int_{LE}^{TE} (c_{pl} - c_{pu}) dx = \frac{1}{2} \rho_\infty V_\infty^2 \int_{LE}^{TE} \frac{c_{pl,inc} - c_{pu,inc}}{\beta} \beta dX = L'_0 \quad (7.6)$$

They are the same, whereas the lift coefficients respect $c'_l = \frac{c'_{l0}}{\beta}$. This is also valid for the lift curve slope.

7.1.2 Supersonic flows

In this case the potential equation becomes:

$$\lambda^2 \hat{\phi}_{xx} + \hat{\phi}_{yy} + \hat{\phi}_{zz} = 0. \quad (7.7)$$

If we apply the analogous transformation we have:

$$X = \frac{x}{\lambda} \Rightarrow \hat{\phi}_{XX} + \hat{\phi}_{yy} + \hat{\phi}_{zz} = 0. \quad (7.8)$$

This equation does not correspond anymore to the equation of an incompressible flow since $\lambda = \sqrt{M_\infty^2 - 1}$ and to have $\lambda = 1$ we need $M_\infty = \sqrt{2}$, thus the new flow is a $M_\infty = \sqrt{2}$. The previously found relations with β are valid for λ .

7.2 Swept wings

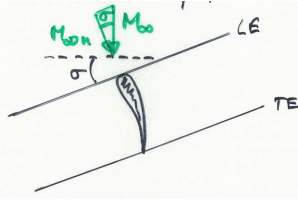


Figure 7.2

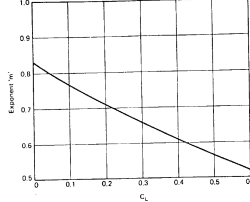


Figure 7.3

This is a technique used in order to increase the critical mach number. Indeed, the flow seen by the 2D wing is the one perpendicular to the wing:

$$V_{\infty n} = V_\infty \cos \sigma \Rightarrow M_{kr}^{\sigma=0} = \frac{M_{kr}}{\cos^m \sigma} \quad (7.9)$$

where we can see that the M_∞ will be higher and where m varying parameter in function of the C_L , it decreases with lift (Figure 7.3). if the sweep angle is large enough, the flow seen by the LE can become subsonic and allow rounded shapes which is advantageous for subsonic speeds. The drag divergence mach number also increases:

$$M_{div} = M_{kr}[1.02 + 0.08(1 - \cos \sigma)]. \quad (7.10)$$

7.2.1 Lift of swept wings

Remind the definition of C_p :

$$C_{pn} = \frac{p - p_\infty}{\frac{1}{2} \rho_\infty V_{\infty n}^2} \quad L_n = \frac{1}{2} \rho_\infty V_{\infty n}^2 \int_{LE}^{TE} (C_{pln} - C_{pun}) dx \quad (7.11)$$

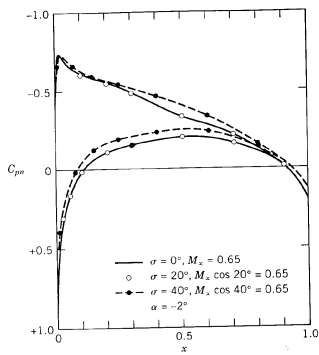


Figure 7.4

where we see that if $M_{\infty n} = M_\infty^*$ (M_∞^* in this case is the one we have without sweep), the pressure distribution and thus the lift remains constant. This means that for a same approaching speed V_∞^* without and with sweep we will decrease the lift (we have to fly at higher speed). The lift coefficient also decreases for $V_{\infty n} = V_\infty^*$:

$$c_l^* = \frac{L^*}{\frac{1}{2} \rho_\infty V_\infty^*} > c_l = \frac{L^*}{\frac{1}{2} \rho_\infty V_\infty} \quad (7.12)$$

where * designate the same value in non swept wing. We see that the lift coefficient decreases.

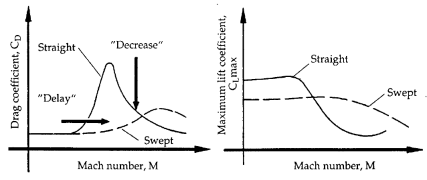


Figure 7.5

Pay attention that this is the case when we are in subsonic flight. Indeed, the sweep increases the lift for supersonic as the shock stall is postponed ($M_\infty n$ seen smaller). In practice, to have significant influence of sweep σ must be high (at least $30^\circ - 40^\circ$).

7.2.2 Lift coefficient as a function of the angle of attack for swept wings

As we have seen, the lift and the lift coefficient decreases when sweep wings. This implies that the slope of the lift curve is also smaller. Remark that we have the same AR in the figure, in practice the AR of swept wing is smaller than the one without (2 to 4 - sweep, 6 to 10 - subsonic), but the lift slope is even smaller.

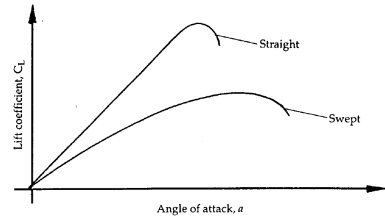


Figure 7.6

There are structural advantages as it allows to have thinner airfoils (better for high speed), and the M_{kr} increases. To increase the structural strength we use **taper** (chord decreases from root to tip). This smaller AR induces more drag, demanding more take-off and landing distance. The reduced slope of lift requires high α when landing and take-off (Concorde drooped nose), but there is no pronounced stall limit.

7.2.3 Influence of the sweep angle on the drag

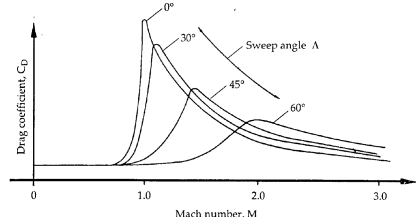


Figure 7.7

One observes the increase of M_{div} , the decrease of the maximum drag coefficient (must have large angles to have significant effects). At sufficiently high Mach numbers, M_n will reach the supersonic limit and produce the same effect as seen previously. In that case, the drag with no swept wing is smaller at this stage.

7.2.4 Some additional disadvantages of wings

Separation behavior

First, remind that the pressure on the suction side decreases moving from the root to the tip, perpendicularly to the flow, inducing a flow. In practice, we try to have the separation at TE the nearest to the root not to disturb the ailerons (or else loose of control). The problem is that as we are already beyond the peak of underpressure at the root, to the tip we reach the underpressure, thus the boundary layer is pushed to the tip, resulting in a flow of low velocity and low energy. This will separate easily.

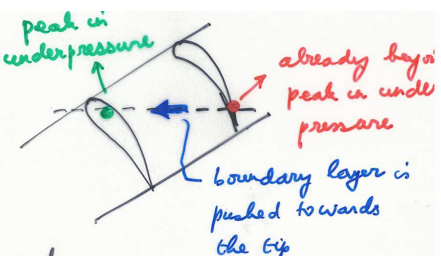


Figure 7.8

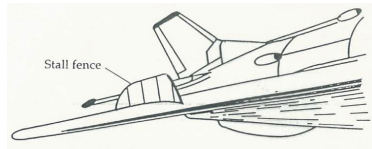


Figure 7.9

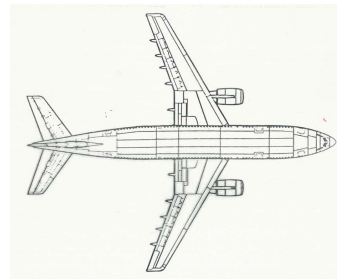


Figure 7.10

Solutions to limit this are:

- **washout:** we make the geometry in order to reduce α when going to the tip and increase the speed.
- **separation at root:** we force it to happen there for example by sharp LE
- **use of slots and slats** (see further)
- **stall fences:** it is a device placed on the wing in order to brake the flow going from root to tip (Figure 7.9).

Efficiency of flaps and ailerons

Flaps are devices made to increase the lift, used in take-off and landing. The flaps become less effective with sweep. For example, a slotted over 60% span can increase the lift coefficient about 50% for non swept and only 20% for swept wings. This is why the part of the wing containing the flaps is not swept.

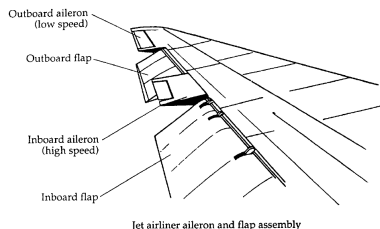


Figure 7.11

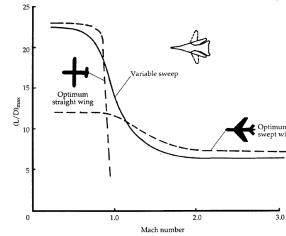
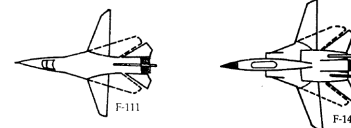


Figure 7.12

Figure 7.13



This reduction of efficiency also occurs with the ailerons. We can conclude that it is better for a plane flying only at subsonic speeds to have no sweep, and better to have sweep for supersonic. We can have a **swing-wing** which is the variable sweep.

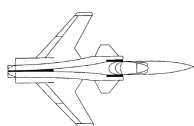
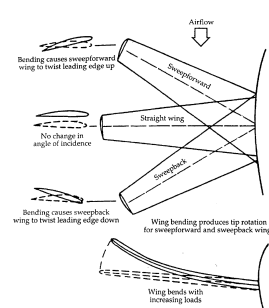


Figure 7.14

The **Forward Swept Wing (FSW)** has the same effect of the aft swept wing (ASW), but has advantages because the separation principle we have seen is reversed such that the separation occurs on the root \rightarrow higher lift. At maximum lift, the FSW has an elliptic lift distribution along the wing, leading to less induced drag than the ASW which has a peak at the tip. This leads to a better efficiency of ailerons and flaps.

But there is a structural instability. Indeed, the load is always accompanied with a bending of the wing. In straight case, there is no rotation of the profile. For the ASW the profile will move downward implying a decrease of the angle of attack (lift) and compensating the bending. In FSW the profile move upward, increasing α and the



lift, causing more bending and so on → unstable. This can be avoided by sufficient structural strength.

Swept wing and supersonic flow

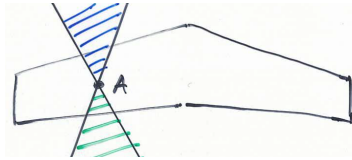


Figure 7.16



Figure 7.17

For high enough speeds, the normal mach number will be supersonic, we'll get **supersonic leading edge**. There will be appearance of the Mach cone, the flow at point A is only influenced by the blue area and it influences the green area. We can go to the tip, we see that it only influences a small part of the wing. The rest of the wing see 2D flow. To avoid the effect of the tip, we cut the region of influence, they are thus inefficient at subsonic and low supersonic speeds

7.3 Area rule

Theorem of Hayes

Within the limits of small perturbations, different planes with the same evolution of the area of their cross section will have the same wave drag at transonic Mach numbers (at zero lift).

Whitcomb

In order to limit the wave drag for transonic flows, the variation of the area of the cross-section of a plane should be as smooth as possible, without abrupt changes.

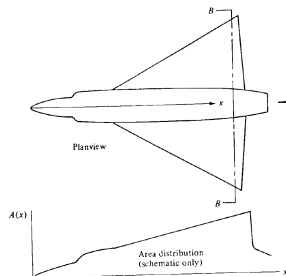


Figure 7.18

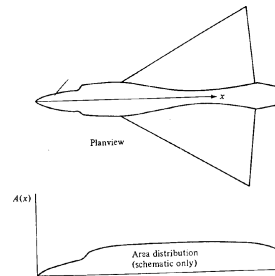


Figure 7.19

This means that the cross section of the fuselage must be reduced near the tail in order to have that smooth variation. On this figure see the decrease and the late of the peak in drag around $M=1$ with area rule.

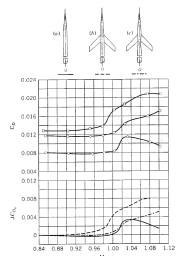


Figure 7.20

7.4 Delta wings

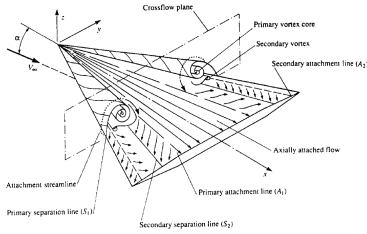


Figure 7.21

The idea of delta wings is to control the separation. By using a sharp LE one obtains a fixed separation line on LE. This is a considerably swept wing but has less problems with tip stall. This is due to the vorticities at the LE on the upper side that avoid the boundary layer to reach the tips. The separation area being limited, that produces an underpressure on the upper side and contributes to lift.

The slope of the lift curve is small, we can reach high $\alpha \approx 35^\circ$.

At still higher α the vorticities will lose their structure (**vortex burst**) and the underpressure will disappear, lift goes down. The large wings produce large lift and flaps are not needed. Tail plane are not necessary and the large chord at the root allows thick wings, keeping t/c low, increasing structural strength, allowing fuel storage and engines integration (reduction of drag). To have good subsonic conditions, $b/l \approx 0.25$ or not smaller than 2.

Remark 1 This description only applies for subsonic LE. If it is supersonic there is no separation at the LE, there is a shock wave on the wing causing boundary layer separation.

Remark 2 The lift creating process is different here. Joukowski theorem tells that it is based on vortex sheet, which is quasi horizontal for traditional wings. For delta wings the vortex sheet is rolled up. For wings with very low AR, c_l in function of α is given by the **formula of Jones**:

$$c_l = \pi \alpha \frac{db}{dx} \quad (7.13)$$

under the assumption that the wing lies perfectly in the Mach cone and where $\frac{db}{dx} = cst$ for delta wings.

Remark 3 The vorticities cause the transition to turbulent flow. If one wants laminar flow boundary layer control is needed.